Numerical Simulations of Airflow in Telescope Enclosures

David S. DeYoung
Kitt Peak National Observatory, NOAO, PO Box 26732,
Tucson Arizona 85726

Gemini Preprint # 17

ABSTRACT

Contemporary design of large telescopes requires optimization of the telescope environment in order to fully realize the capabilities of advanced mirror technology, telescope control and instrumentation. Telescope enclosure design is a critical element in providing this optimized environment. Enclosures must protect the telescope while minimizing the local degradation of image quality, and the large cost of such structures requires that a successful design be in place before construction begins. In order to test various enclosure designs, three dimensional non-linear hydrodynamic calculations have been carried out to determine the flow of air within and around proposed enclosure configurations. Such calculations can test the effectiveness of dome venting, evaluate the dynamic pressures that cause possible deformation of primary mirror surfaces and structural windshake, and isolate sources of turbulent flow that may cause image degradation. Results are presented from a series of calculations that investigated characteristic flows in the Gemini 8-meter enclosure and around its associated primary mirror cell. In general the enclosure design is found to meet its overall design goals. Good dome venting is achieved under a variety of conditions, yet the telescope structure is kept in a low wind environment.

1. INTRODUCTION

Optical astronomy is currently undergoing a revolution in capability with the proliferation of 10 meter class telescopes worldwide. These facilities incorporate highly sophisticated technology in terms of mirror fabrication and control, telescope design, pointing and tracking control, instrumentation, and data analysis and reduction (e.g., Stepp 1994). Coincident with the high degree of technical development evident in these facilities is their very high cost. These large levels of expense imply that as much care as possible be exercised in the overall design and placement of these facilities, which in turn requires that as much problem solving as possible be done before actual fabrication begins. One critical factor that can undo much of the technical sophistication in the telescope design is an environment that results in poor seeing. (Throughout this paper the term "seeing" will be used as a general description of image quality; the term "poor seeing" is thus equivalent to image degradation.) Image degradation that is independent of telescope design can come from two sources: placement of the telescope on a site which produces less than ideal seeing due to large scale topological or meteorological conditions, and local degradation of seeing in the immediate telescope environment due to inadequate removal of heat sources in the enclosure or improper circulation of air within the enclosure. Ideally these conditions should be minimized before site selection and fabrication. Another aspect of air circulation within an enclosure involves wind loading on the telescope and on the mirror itself; again in the ideal case these deformations would be known in advance and compensated for in the final telescope design.

Past attempts to solve these problems, all of which involve the interaction of the telescope with its environment, have been approximate, empirical and even anecdotal. Empirical solutions require expensive experimental programs, especially if the correct scale is to be employed and if a large volume of parameter space is to be sampled. For example, test facilities employing wind loading on telescope structures would need to be nearly full scale and able to produce a wide variety of wind conditions in order to obtain useful results, and sampling temperature variations throughout the interior of proposed telescope enclosures under various wind conditions would also be an expensive program. For problems of this nature that involve fluid flow in and around various structures an effective and much less expensive set of solutions can often be found

through the use of numerical simulations or computational fluid dynamics (CFD). The CFD approach permits arbitrarily large variations in ambient conditions and a wide variety of test designs to be placed in these conditions. The 3D calculations can be fully nonlinear and thus can examine the role of dome flushing, turbulence and the resultant effect on seeing, as well as providing wind speeds, directions, and dynamic pressures to serve as input to telescope and mirror support structural designs.

This technique has recentlv been used to examine the effects of both large scale and local topography on seeing at proposed telescope sites (De Young and Charles 1995). Such studies have provided useful input into site selection criteria and global telescope design considerations such as the height of the telescope above ground level. These same methods are used here to address two additional issues, namely the airflow through proposed enclosure designs and the wind loading on mirror support structures. Numerical simulations can be viewed as a valuable supplement to water tunnel tests. Water tunnel experiments can incorporate more complex geometries than can realistically be included in numerical simulations, but because of their small scale it is difficult for these experiments to reproduce flows at Reynolds numbers that correspond to the actual structures being designed. CFD techniques do not suffer from this restraint, and calculations that employ the correct range of Reynolds number flows will allow a direct comparison with water tunnel results to see if significant differences exist between the two techniques.

The fundamental issue is the degradation of image quality, and this in turn is primarily a result of the mixing of air parcels at different temperatures which are then advected into the line of sight. (Because the flow velocities are very much less than the sound speed, pressure fluctuations are negligible and not a serious source of image degradation; i.e., the flow is essentially incompressible, so that index of refraction changes due to density fluctuations can be ignored.) Processes directly related to this air parcel advection are the effectiveness of dome air flushing to achieve a nearly isothermal interior and the presence of large scale turbulent structures. It is important to note that for Reynolds numbers appropriate to airflow through telescope enclosures ($R_e \sim 10^6$-10^7) the flow is in the fully turbulent regime. Turbulence per se is not a source of image degradation if the flow is fully isothermal and incompressible. However, if

the enclosure is poorly flushed and contains regions of air at different temperatures, then turbulence can mix these different regions and contribute to image degradation. Conversely, in some instances the onset of turbulence can actually be beneficial if it promotes the removal of stagnant volumes of air and improves the overall dome flushing. A final consequence of turbulence lies in its effect on the power spectrum of energy contained in the airflow impinging on the telescope enclosure. In general turbulence can shift energy in the power spectrum from lower to higher frequencies, and this in principle can move low frequency power into the range of a few hertz to a few tens of hertz. This range can cause problems for telescope control systems at the low end and can excite resonances in the telescope structure at the upper end. However, this effect is significant only if most of the volume in the telescope enclosure is characterized by the presence of well developed turbulence; otherwise the total power shifted to higher frequencies is not critical. The calculations presented here were carried out in conjunction with the design and development of the two 8-meter telescopes being constructed under the Gemini Project. This international collaboration involves the United States, Canada, the United Kingdom, Chile, Brazil and Argentina in a joint effort that will place one telescope on Mauna Kea in Hawaii and one telescope on Cerro Pachon in Chile (Mountain et al. 1994).

Thus the goals of the current set of numerical studies were the following. To examine the airflow in and around proposed telescope enclosures in order to determine: 1) the effectiveness of dome vents in allowing ambient air to "flush" the interior and thus provide good thermal control and removal of warmer than ambient air; 2) to see how much turbulence was created inside the dome under a variety of wind speeds and directions; 3) to evaluate the protection against wind loading and wind shake provided by the enclosure. The wind loading is of particular importance at the upper end of the enclosure in the area of the telescope secondary due to the long moment arm relative to the rotational bearings of the telescope near its base. An additional goal was to determine the distribution of pressure across the mirror and its support structure under a variety of wind speeds and directions. In what follows Section 2 provides a detailed description of the initial and boundary conditions for the problems examined, together with a brief outline of the method of calculation. Section 3 then shows a sampling of the results and their impact, and concluding remarks are given in Section 4.

2. BOUNDARY CONDITIONS AND METHOD OF CALCULATION

2.1. Telescope Enclosure

One of the major issues in the enclosure design involved the use of vents in the walls of the structure. The vents will provide movement of large volumes of ambient air through the enclosure, and this facilitates cooling the dome and telescope down to ambient air temperatures was well as removing warm air produced by heat sources within the dome. However, vents that are too large or that are poorly placed can also introduce turbulent wakes at their edges which can degrade image quality. In addition excessive venting might permit undesirable wind loads to be placed on the telescope structure, especially near the secondary. Thus the issue if venting is one of extent and location, and the CFD calculations examined two proposed enclosure designs with different degrees of venting. Figure 1 shows a drawing of these designs; two options for venting were considered as shown in the figure, but the major focus was on the configuration depicted in the upper right. The computation requires a numerical mesh to be generated that represents the enclosure, and this three dimensional mesh is then placed in a rectilinear volume which is also subdivided into small volume elements. These calculations do not include any representation of the telescope structure within the enclosure; inclusion of such substructure would require a mesh of enormous complexity and size that would demand impractical amounts of computer memory and CPU time. All values of the flow variables (velocity, pressure, etc) are calculated in each volume element and at each point on the surface mesh that models the enclosure. Figure 2 shows some sample views of the mesh used in the calculations. Although the geometry depicted is rather simple, a large number of elements are required to obtain an accurate result. This is particularly true for turbulence modelling, which require high resolution near any solid surfaces. In this case the overall dimensions of the calculational volume is 260 meters, with an enclosure diameter of 36 meters, yet the size of the volume elements next to the solid surfaces is only 6 cm. The total number of mesh elements used in the computational domain shown in Fig. 2 is 103,565, with over 2.6 million matrix elements used in the calculation.

The flexibility of CFD allows any number of wind speeds and directions to be used in examining flow through the structure, but the large scale of the computation restricts the total

number of cases that can be calculated. Each solution required approximately 7 to 9 hours of CPU time on the Cray C90 at the San Diego Supercomputer center. Wind directions were varied between the extremes of the telescope facing directly into the wind and with the telescope at right angles to the wind. Wind speeds varied between 3 and 11 m/s. The lower value was taken to examine the effectiveness of venting in light winds, and the higher value, which is the 70th percentile value on Mauna Kea, was taken to examine the effects of turbulence and wind loading. Boundary conditions permitted uniform inflow or unconstrained outflow along any of the outer walls of the volume, and the wind speed was set equal to zero on all solid surfaces. A free slip condition with no outflow was used along the top of the volume. The vertical extent of the volume was taken to be far enough above the top of the enclosure so that no boundary effects were present at the enclosure itself. The same criteria were used for the distance of the upstream and downstream boundaries. The upstream boundary must be far enough away that the flow has established a self consistent boundary layer along the ground by the time it reaches the enclosure, and the downstream boundary must be far enough from the enclosure that any wake vortices can close before reaching the boundary. In all cases the ambient air density was taken to be that of a standard atmosphere at 4300 meters msl. The calculations are isothermal and incompressible, which is appropriate for the flow speeds used here.

2.2. Mirror and Ceil Structure

A separate mesh was used to examine the flow and around, and pressure patterns on, the mirror and its cell. This permits a larger scale to be used to obtain the required resolution for the various pressure distributions. Similar considerations exist for the initial and boundary conditions here as for the more complex mesh used in the enclosure simulations. In this case the mirror and its backup structure were represented by a simple right circular cylinder, and it is clear from symmetry considerations that only one half of the cylinder and its surrounding volume need be used in the actual calculations. The diameter of the mirror cell was set at 9.0 meters, and its thickness was set at 3.0 meters. A total of 103 257 mesh elements were used in the calculation, and a representative view of the mesh is shown in Figure 3. Wind directions were varied from 90 degrees (mirror facing directly into the wind) to 0 degrees (wind blowing directly across the mirror), and wind speeds were taken to vary from 2 m/s to 11 m/s. In each case the incident wind

flow was laminar and did not include any upstream turbulence that could be introduced by the telescope structure. The presence of such turbulent flow is unlikely to introduce major changes in the time averaged pressure distributions from those of the laminar flow case. Each calculation required approximately 9 hours of CPU time on a Cray C90 because of the high resolution required.

2.3. Method of Calculation

As mentioned above, the calculations are fully three dimensional, incompressible and time independent. Because the design considerations are aimed at average or most common conditions, steady state calculations are most appropriate. For the wind speeds used here, compressibility is not a factor, and as mentioned in Section 1, the calculations can adequately represent flows with the very high Reynolds numbers needed. The value of the Reynolds number is given by Re = UL/v where U is a characteristic speed, L is a characteristic length scale (e.g., the size of the enclosure) and v is the kinematic viscosity. Values of Re appropriate for these problems lie in the range 106 to 107. The specific numerical method used is that of finite element analysis, and the software is essentially the same as was used by De Young and Charles(1995). A more detailed discussion of the numerical techniques. including the treatment of turbulent flow, can be found in that reference .

3. RESULTS

3.1. Overview

Large three dimensional calculations such as these generate extremely large amounts of data, and care is needed to provide results in a comprehensible and easily understood way. The primary flow variables that are of interest for evaluation of telescope enclosure designs are the velocity field, the vorticity $\omega = \Delta \times \mathbf{v}$ and to a lesser extent the pressure. For wind loading on the mirror cell the primary diagnostic is the pressure, with the velocity and vorticity being secondary indicators. The vorticity provides a direct measure of turbulence and mixing. From its functional form one can see that any shear layer which involves velocity gradients normal to the mean velocity, such as occurs in flow over any solid surface, will result in a nonzero vorticity in that

region. Similarly, any turbulent wakes which involve rotational flow or eddies will also cause nonzero vorticity. Thus Id is a good measure of areas in the flow that can cause degradations in seeing if there are any variations at all in the air temperature (which will almost always be the case).

In general the diagnostics will be in the form of plane cuts through the three dimensional volume parallel to one of the major axes. When velocity vectors are displayed the plane contains the projection onto that plane of the full three dimensional velocity vector and not just the velocity components that lie in that plane. In addition to velocity vector planes, the other major components displayed will be the magnitude of the velocity in the plane, $u = \left[u_x^2 + u_y^2 + u_z^2\right]^{1/2}$ the magnitude of the vorticity, $w = \left[w_x^2 + w_y^2 + w_z^2\right]^{1/2}$ and the pressure.

3.2. Flows Through Telescope Enclosures

As described above, several different Calculations were made for two different geometries and several different wind directions and speeds. Often the most effective way to display complex data sets is through extensive use of color; due to the expense of color reproductions only a sample of the results will be presented here, although the salient results for the entire package of simulations will be described. Examples will be given for flow conditions through the enclosure shown in Figure 1 and for the limiting cases of wind speed and direction, namely speeds of 3 and 11 m/s and directions either perpendicular to the telescope major axis or parallel to its projection on the ground plane.

Figure 4 shows the airflow through the enclosure in a horizontal plane that contains the mirror surface, with the wind passing through the vent openings in a direction perpendicular to the telescope's optic axis. The vectors shown are for a high wind speed of 11 m/s; it is important to note that in this and all subsequent velocity vector plots the positions of the vectors are NOT along flow streamlines. The base of each vector is located at the center of a computational volume in the grid. Thus the distribution of vectors reflects the grid structure, not the streamlines of the flow. This figure reveals an important positive aspect of the flow through the enclosure with the vents open, namely that the flow is smooth on large scales in the center of the enclosure

where the telescope primary mirror is located. Although the vector crowding makes resolution difficult in some areas, it is clear that the scale of turbulence created at the edges of the vent walls does not seem to propagate into the central region. Another feature is the reduction in wind speed in the interior below the free stream value of 11 m/s. These aspects are also shown clearly in Figure 5. which is a color rendition of the magnitude of the velocity (speed). The color stretch used here is set to emphasize variations in the lower speed regime, hence the reduction in velocity at the center over ambient is not as evident as in Figure 4. However, Fig. 5 does clearly show the effects of the edges of the vents and shows that at this high wind speed the turbulence generated by these edges does not propagate into the region occupied by the primary mirror. The asymmetry in the wake flowing past the enclosure in Fig. 5 is due to the effects of the asymmetry in the vent structure and to a lesser extent to the presence of the telescope opening shown in outline on the centerline of the structure.

At these high wind speeds and with the wind flowing directly through the vents, a natural concern is the wind speed at the top end of the telescope, where relatively high wind speeds could produce undesired wind shake. This issue is addressed in Figure 6, which is a color rendition of wind speed in a horizontal plane that passes through the mirror secondary. The geometry shown here is for the telescope pointing at a zenith angle of 40 degrees (cf Fig. 1), which places the secondary rather high in the telescope enclosure. This figure clearly shows the shielding of the top end provided by the enclosure. The shape of the enclosure provides a deflection of the high speed flow past the opening for the telescope light path, much in the same way that a small motorcycle windshield will deflect airflow over the rider. There is some outflow of air from the interior as can be seen in the figure, but the speed of this flow is low, with a small maximum at the aperture itself due to the Bernoulli effect. The wind speed in the center of the enclosure at the location of the secondary is quite low, thus reducing the effects of windshake. The outflow of slowly moving air from this aperture also shows that the entire dome is being flushed with ambient air and that heat removal should be effective. Another view of the interior flow in this case is shown in Figure 7, which is a vertical cut through the center of the enclosure in a plane parallel to the ambient wind. The color stretch here clearly shows the deceleration of the ambient wind inside the enclosure, in contrast to Fig. 4, and the expected upstream

deceleration is also clearly shown. The speedup of the flow as it passes over the curved upper surface of the enclosure is also seen, a verification of Bernoulli's theorem. Figure 7 also shows the low speed region in the upper portion of the enclosure interior, showing that this design provides good protection against windshake at relatively high wind speeds.

A second set of calculations addressed the issue of dome flushing at low wind speeds. Figure 8 shows the velocity vectors for a wind from the same direction as discussed above but with an ambient wind speed of 3 m/s. The horizontal plane is the same as used in Fig 4, namely that which contains the primary mirror. Fig. 8 shows a velocity field very similar in overall geometry to that of Fig. 4, though many differences in detail exist. Note that the length of the vectors in these two figures is normalized to the same value for the ambient upstream wind; this is to provide the optimum resolution in each figure. The average wind speed near the center of the enclosure in this plane is about one m/s, thus an estimated flushing rate in this region is approximately two volume changes per minute. Thus Figure 8 shows that at low wind speeds there is again good transfer of air and heat out of the dome, and equally important, the effects of the vent edges do not disturb the flow near the center. Figure 9 shows the distribution of wind speeds in the interior in a manner similar to Fig. 7. Good movement of air is shown throughout most of the enclosure interior, with minimal velocities near the top end of the telescope.

Another case of obvious interest is for wind directions perpendicular to the main vents when the telescope is facing directly into the wind. Figure 10 shows the velocity field in the primary mirror plane for this case with a wind speed of 11 m/s. It is clear now that there is considerably less wind flow across the primary than for the case shown in Fig. 4. Moreover, large turbulent vortices are evident in the interior inside the edges of the vents, though it does not seem that this turbulence propagates to the center of the enclosure where the primary is located. These turbulent structures can possibly create a stagnation region near the enclosure wall; it is not clear from the simulations how rapidly air will diffuse out of this region. This isolation of the vortices is verified by Figure 11, which shows the distribution of speed in this plane. Though strong velocity gradients exist, the central region of the enclosure appears to be characterized by a uniform low velocity flow. Examination of the velocity vectors in Fig. 10 shows that is flow in the central region is of order 1 m/s, which at two volume changes per minute is adequate to remove warm air

generated by any heat sources and to bring the enclosure interior into thermal equilibrium. An accurate measure of the turbulence induced by the vents comes from examining the vorticity, and Figure 12 is a color map of the magnitude of the vorticity in the mirror plane for this flow. Comparison with Fig. 11 clearly demonstrates sensitivity of vorticity maps to determining the location of turbulent flows. The results from this figure are encouraging in that the level of vorticity at the center of the enclosure is very low, implying that even if the uniform flushing does not result in an isothermal flow at this location, turbulent degradation of images will not be a major problem across the mirror face in this case. (In actuality some small scale turbulence will be induced across the mirror by the presence of nearby telescope structural members.)

A high wind speed of 11m/s, with the telescope aperture facing into the wind, naturally gives rise to concerns about wind entering the top end of the enclosure and causing excessive wind shake. Figure 13 shows the velocity field in the plane containing the secondary in this case. Though there is clearly some inflow, the wind speed is significantly reduced to speeds of 2 - 3 m/s from 11 m/s. This is again due to the flow deflection discussed above, and Figure 14 shows this clearly. This color map of speed in the vertical plane parallel to the wind vector shows some increase in wind speed near the telescope aperture, but in general the upper region of the enclosure remains characterized by uniform and low speed flow. The actual turbulence generated by the wind impinging upon the telescope aperture is depicted in Figure 15, which displays the magnitude of the vorticity in the interior of the enclosure in the same vertical plane. Turbulence is clearly present in and near the aperture, and if any thermal gradients are present then this turbulent layer will degrade the seeing, as the light path must pass directly though it. However, the vorticity is largely damped out in the center of the enclosure, and thus turbulence induced wind shake should not be a significant problem in this configuration.

No simulations were performed with the wind impinging on the "back" of the enclosure so that the telescope is looking though its wake, since the primary concern was to determine flow patterns within the dome itself. However, examination of the vector fields in a vertical plane through the enclosure centerline shows that the enclosure wake is characterized by a closed vortex that forms immediately behind the structure. This vortex extends from the ground up to about two thirds of the total height of the enclosure, and its presence indicates that air is mixed

from the ground level through the major portion of the wake. Given that ground temperatures often differ markedly from air temperatures a few meters above the ground, this would imply that significant image degradation could occur when the telescope is at low elevation angles and is looking through its own wake.

It is important to note that the flow geometry shown in Figures 10-15 was also tested in experimental water tunnel measurements. Some of the results of that experiment have been documented in the Gemini Critical Design Review report (1994), and more complete reports are found in Siegmund et al. (1990) and in Forbes et al. (1991). Although the flow speeds and Reynolds numbers in the water tunnel test are very different from those used here, the overall flow patterns are very similar. In particular, the water tunnel tests found wake mixing in a manner akin to that hinted at by these simulations, and they also found a rising pattern of streamlines upstream of the enclosure which is also seen here. This experimental agreement with the computations, together with the demonstration in the computations of well known and expected phenomena such as the Bernoulli effect, all provide encouraging confirmation of the accuracy of the calculations. Conversely, the agreement between the CFD results and the water tunnel tests may be taken as evidence at the difference in Reynolds numbers used in the two methods does not drastically alter the overall results.

The figures shown above are a small sample of the results available from the modelling of airflow inside the proposed telescope enclosures. In general the adopted design provides good venting of the interior under low and high wind speeds from all directions, yet at the same time the enclosure provides good protection near the top end of the telescope so that wind induced deformation and shake is kept to a minimum. Table 1 shows the effectiveness of wind flushing at the mirror surface under the range of conditions simulated. It is interesting to note that the calculations do not simply scale with different wind speeds when complex geometries are involved. This is not a surprising result for such turbulent, high Reynolds number flows and is another confirmation of the need to perform accurate three dimensional Calculations in order to obtain reliable results. The problems of turbulent degradation of image quality remain for orientations that require the telescope to look into the wind. However, this phenomenon will be present in all telescope enclosures, and it is interesting to note that the turbulent layer shown in

Fig 15 is rather thin. It would be of interest to determine the thickness of this layer produced by existing telescope enclosures.

3.3. Dynamic Pressure on Mirror Structures

The final aspect of airflow and telescope environment considered in these calculations involved the pressure loading of the primary mirror under various wind speeds and directions. This information is of essential importance in designing mirror support structures and active optics elements. The computational mesh for these calculations is shown in Figure 3. Wind speeds varied from 2 m/s to 11 m/s, and flow solutions were calculated for wind directions relative to the mirror surface of 0, 30, 60, and 90 degrees. Sample results from two runs will be shown here, namely for wind directions of 30 and 60 degrees to the mirror surface and for wind speeds of 11 m/s.

Figure 16 shows the flow field across the mirror structure in a plane parallel to the ambient wind for the case of 30 degree incidence, and Figure 17 shows the corresponding velocity field for the case of 60 degree incidence. The presence of vortex structures at the edges of the mirror cell is clearly evident, and the increase in strength of these structures as the angle is increased is also easily seen. one would expect such vortices to be associated with lower pressure, and that is in fact the case as can be seen in Figure 18. This figure shows the pressure fields in the same plane as Figs. 16 and 17, and the strong areas of low pressure are clearly evident as are the high pressure regions. The low pressure on the backside of the support structure must be considered in evaluating deformations of such structures with various wind conditions.

Finally, Figure 19 shows the pressure distributions on the front surface of the mirror for these two wind conditions. It is very clear that strong pressure gradients exist on this surface for both cases and that the resultant forces will produce distortion of the primary unless proper compensation is introduced into the mirror support design. Variations in pressure across the mirror surface exceeded factors of three in some cases, such as the 30 degree case shown here. The quantitative results from these calculations were provided as input during the Gemini mirror support design phase. As in the case of airflow in telescope interiors, some experimental data

have been gathered for pressure forces on mirror surfaces. Noethe et al. (1992) performed measurements of wind pressures on a 3.5 meter model blank at La Silla for VLT design studies. Although their primary interest was the implementation of active optics, where comparable their data are consistent with the numerical simulations made in these studies.

4. CONCLUSIONS

State of the art computational fluid dynamics software, when coupled with the speed of current supercomputer hardware, can provide valuable insights into airflow in and around telescope structures and enclosures. The results of these calculations can be used to evaluate and modify telescope structures early in the design phase, thus making possible considerable cost savings. Numerical simulations are much less expensive to carry out than large scale experimental projects, and because of their ability to solve flows at very large Reynolds numbers with a wide variety of parameters they provide an ideal complement to water tunnel tests.

In the case of the enclosure design for the 8m Gemini Project, the proposed enclosure design was shown in advance to provide mostly uniform flow throughout the enclosure volume under a variety of conditions, with good protection from windshake at the top end at all times. Dome venting was most effective for wind directions most nearly through the vents and perpendicular to the telescope major axis, and in this case venting was good even at very modest wind speeds. Turbulence across the telescope aperture is present in all cases, but is worst when the telescope in facing directly into the wind. However, in all cases the turbulent boundary layer is rather thin, and thus the seeing degradation may be minimal. The results at different wind speeds do not scale directly, and hence the full calculations must be made for all relevant values of the parameters in order to obtain useful results.

Calculations of pressure distributions across the mirror surface and its backup structure under a variety of wind conditions reveal that strong pressure gradients exist on the mirror surface, and these must be compensated for in the support design. In addition, strong low pressure regions are formed along the sides and baek of the support structure, and these deforming forces must also be considered in the design of the mirror support and its compensating mechanisms.

The use of numerical techniques in future telescope design is continuing. Studies of the effects of temperature differences are currently underway, as are the effects of modifying existing telescope enclosures. These modifications are very expensive, and it is desirable to have an accurate estimate of their effect in order to make informed decisions about future allocation of resources. These techniques can also be used to evaluate designs for new state of the art facilities that require active air control over mirror surfaces, such as the proposed CLEAR telescope for solar astronomy.

Thanks are due to an anonymous referee for many useful comments. The numerical simulations reported here were carried out at the San Diego Supercomputer Center, and thanks are due to the SDSC staff for their generous assistance. Thanks are also due to Richard Charles for software consulting and to Dr. Nigel Sharp for assistance with aspects of the postprocessing.

REFERENCES

De Young, D.S. and Charles, R.D. 1995, AJ 110, 3107

Forbes, F., Wong, W-Y., Baldwin, J., Seigmund, W., Limmongkol, S., and Comfort, C. 1991, SPIE Proc 1532, 146

Mountain, M., Kurz R., and Oshman, J. 1994, SPIE Proc.,2199,41

Noethe L., Mornhinweg, M., Ravensbergen M., Sarazin, M., Timmerman, G., and Zago, L. 1992, ESO Technical Report "Pressure measurements with a dummy mirror and the implications for the design of the enclosure and support of the primary mirror of the VLT"

Siegmund, W.A., Wong, W-Y., Forbes, F., Comfort, C., and Limmongkol, S. 1990, SPIE Proc 1236, 567

Stepp, L. 1994, in Advanced Technology Optical Telescopes V, edited by L. Stepp, SPIE Proc. 2199 (SPIE, Bellingham)

This manuscript was prepared with the AAS LaTeX macros v4.0.

Fig. 1.—Three view drawing of the telescope enclosure modeled here. Shaded areas denote openings in the enclosure. The two front views on the right show two separate configurations simulated; effort was largely focussed on the configuration shown in the upper right. The enclosure is 35.4 m in diameter, and the aperture for the light path to the telescope is 9.5 m wide. The side vents are l0 m high.

Fig. 2.—a: Perspective view of the computational mesh containing the enclosure model. The downstream distance between the enclosure and the boundary of the volume is larger than the upstream distance to allow vortex closure. The top of the mesh is flat; the change in mesh size creates the illusion that it is not. b: Close up view of the enclosure model and surrounding fluid mesh. "Stray" lines are due to errors in the projection software.

Fig. 3.—a: Outer mesh definition for the simulations of airflow over mirror cells. A partial set of mesh points for the cell itself are shown in the center. b: Computational mesh array on the surface of the mirror.

Fig. 4.—Velocity field in a plane containing the mirror surface near the floor of the enclosure. Telescope opening is shown in outline on the right side, and the main vents are at the top and bottom. Velocity vectors are placed at the centers of mesh volumes, not along streamlines.

Fig. 5.—Color map of the distribution of wind speed for the case shown in Fig. 4

Fig. 6.—Color map of the wind speed in a horizontal plane containing the mirror secondary. Note the low interior velocities and low speed outflow.

Fig. 7.—Color map of the wind speed interior to the enclosure in a vertical plane parallel to the ambient wind and passing through the center of the enclosure.

Fig. 8.—Velocity field for the same plane and wind direction shown in Fig. 4 but with an ambient wind speed of 3 m/s. Maximum velocity vectors are normalized to the same length in Figs 4 and Fig 8.

Fig. 9.—Color map of the wind speed for the same plane as in Fig. 7 but with a wind speed of 3 m/s

Fig. 10.—Velocity field in the plane containing the primary mirror for a wind directed into the telescope opening at 11 m/s.

Fig. 11.—Color map of the wind speed for the flow field shown in Fig. 10.

Fig. 12.—Color map of the distribution of vorticity for the flow shown in Fig. 10.

Fig. 13.—Velocity vectors in the horizontal plane containing the secondary for wind flow directed into the telescope opening at 11 m/s. Note the low internal wind speeds.

Fig. 14.—Color map of the wind speed interior to the enclosure for a wind directed into the telescope opening at 11 m/s.

Figs 15.—Color map of the vorticity distribution of the flow shown in Fig. 14.

Fig. 16.—Velocity field around the mirror and cell for a wind of 11 m/s directed at 30 degrees to the mirror surface.

Fig. 17.—Velocity field as in Fig. 16 but for a wind direction of 60 degrees to the mirror surface.

Fig. 18.—a: Pressure field around the mirror and cell for the flow shown in Fig. 16. The sharp edge in the red high pressure region is an artifact of gridding and the color stretch in the postprocessing software. b: Pressure field for the flow shown in Fig. 17.

Fig. 19.—a: Pressure distribution on the mirror surface produced by the flow shown in Fig. 16. b: Pressure distribution produced by the flow shown in Fig. 17.

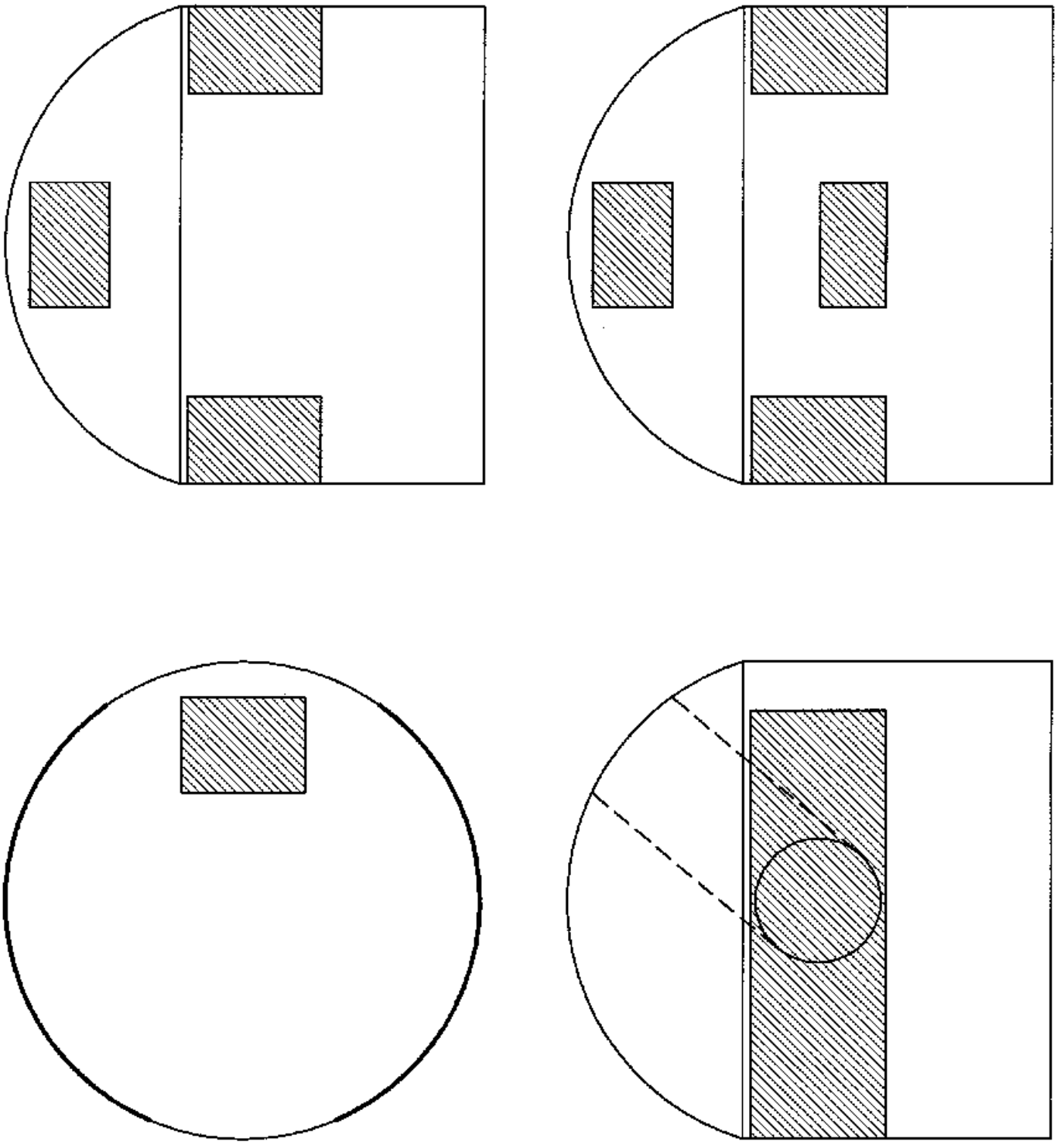

1

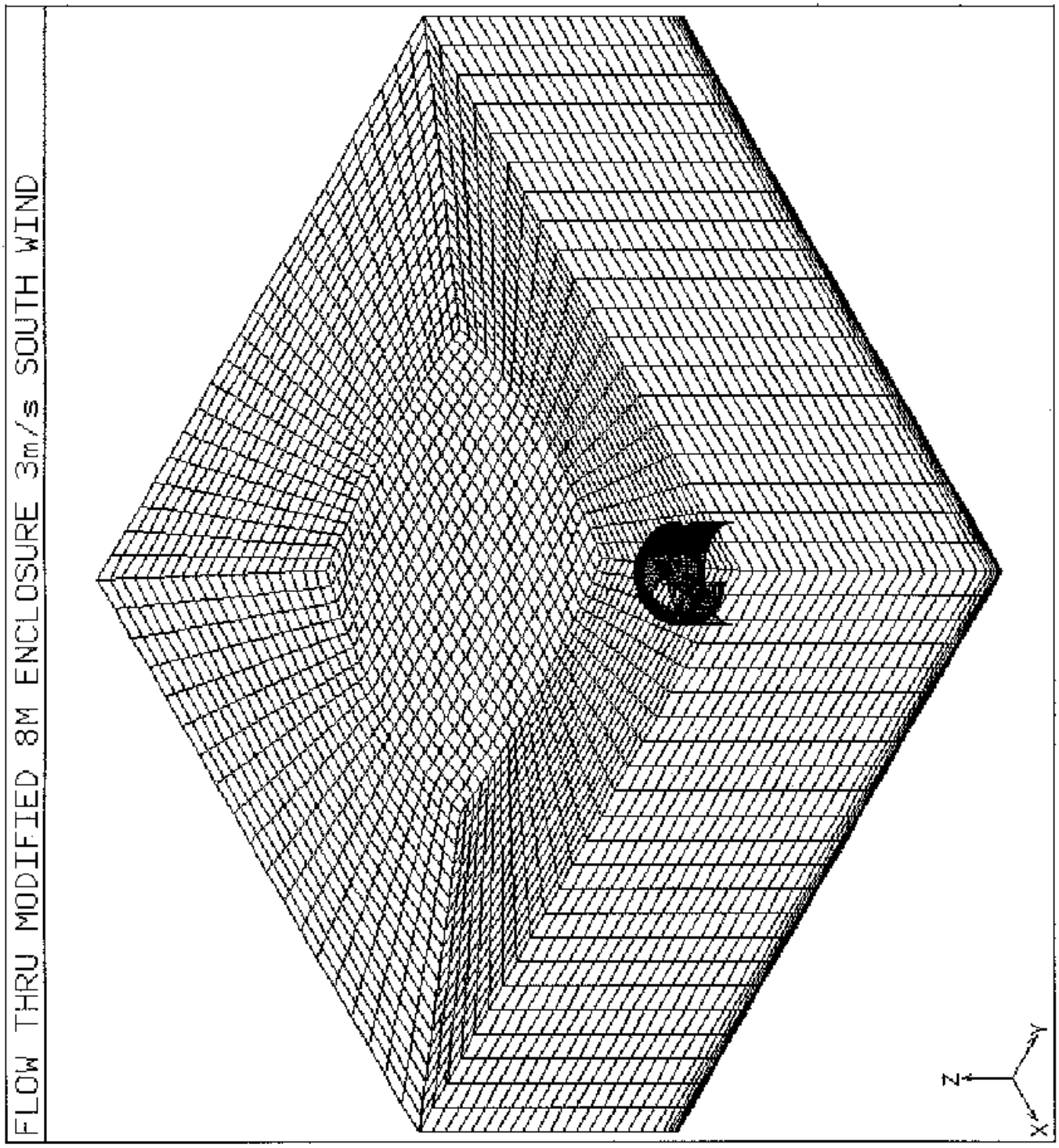

2a

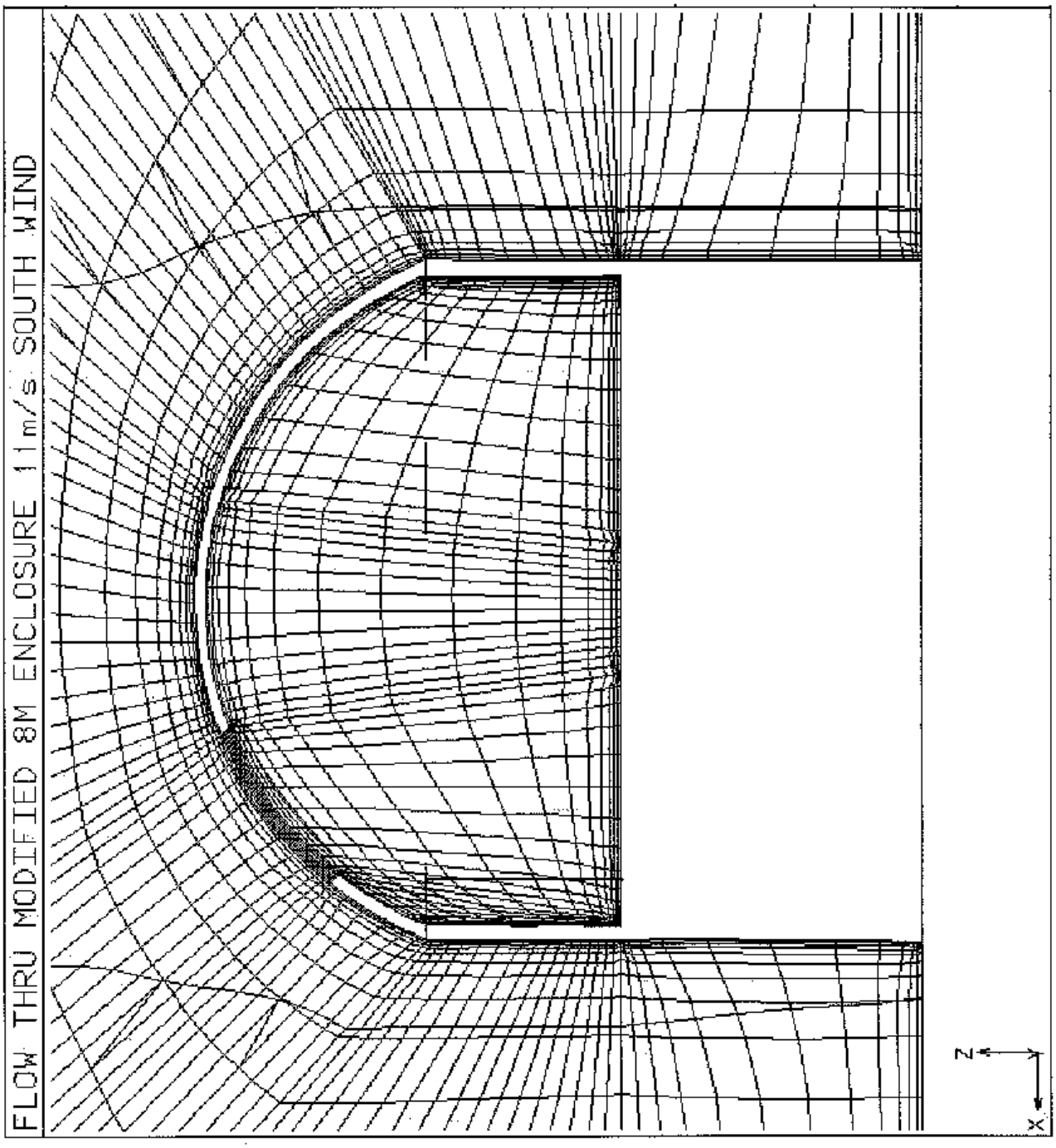

2b

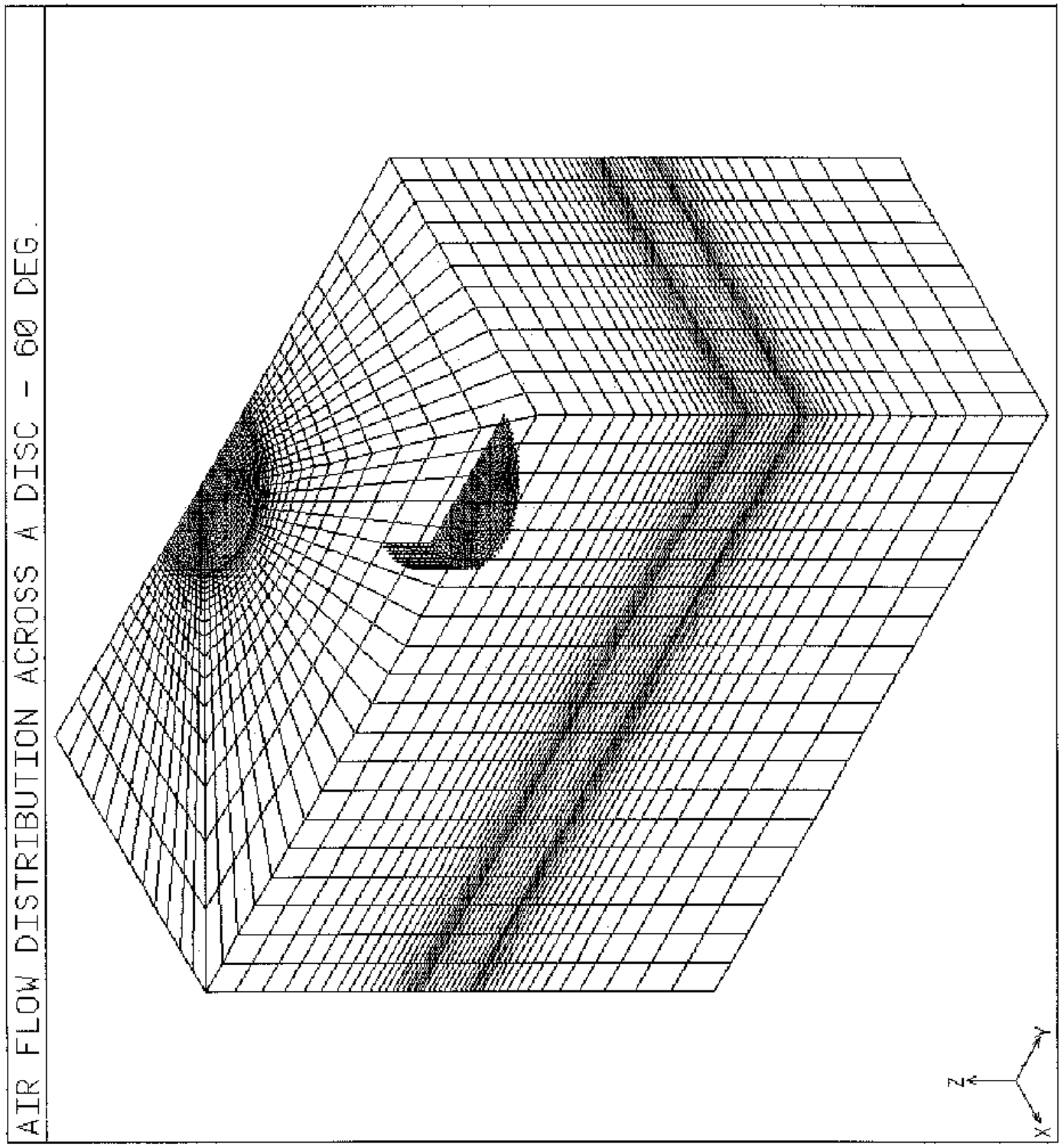

3a

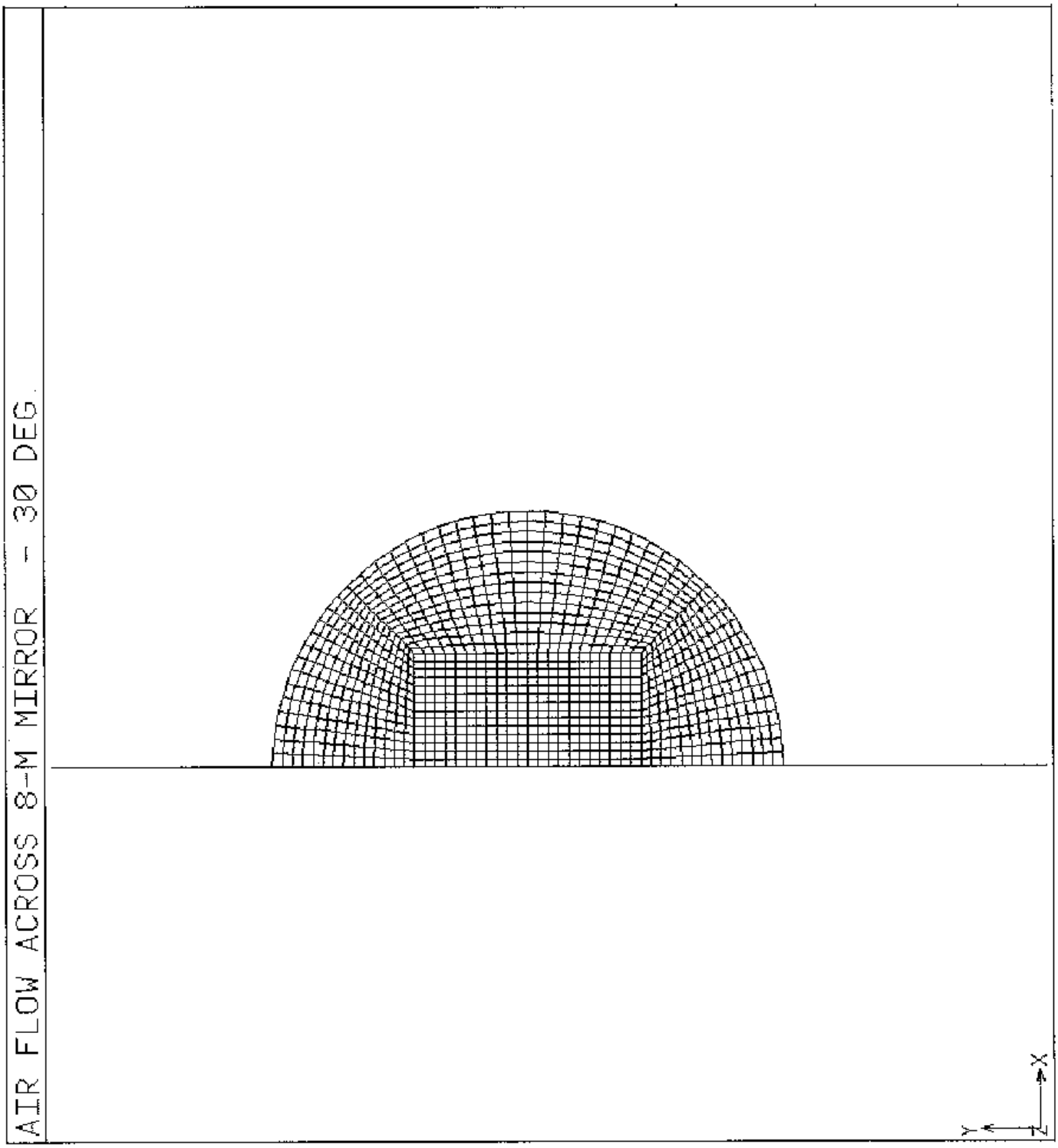

3b

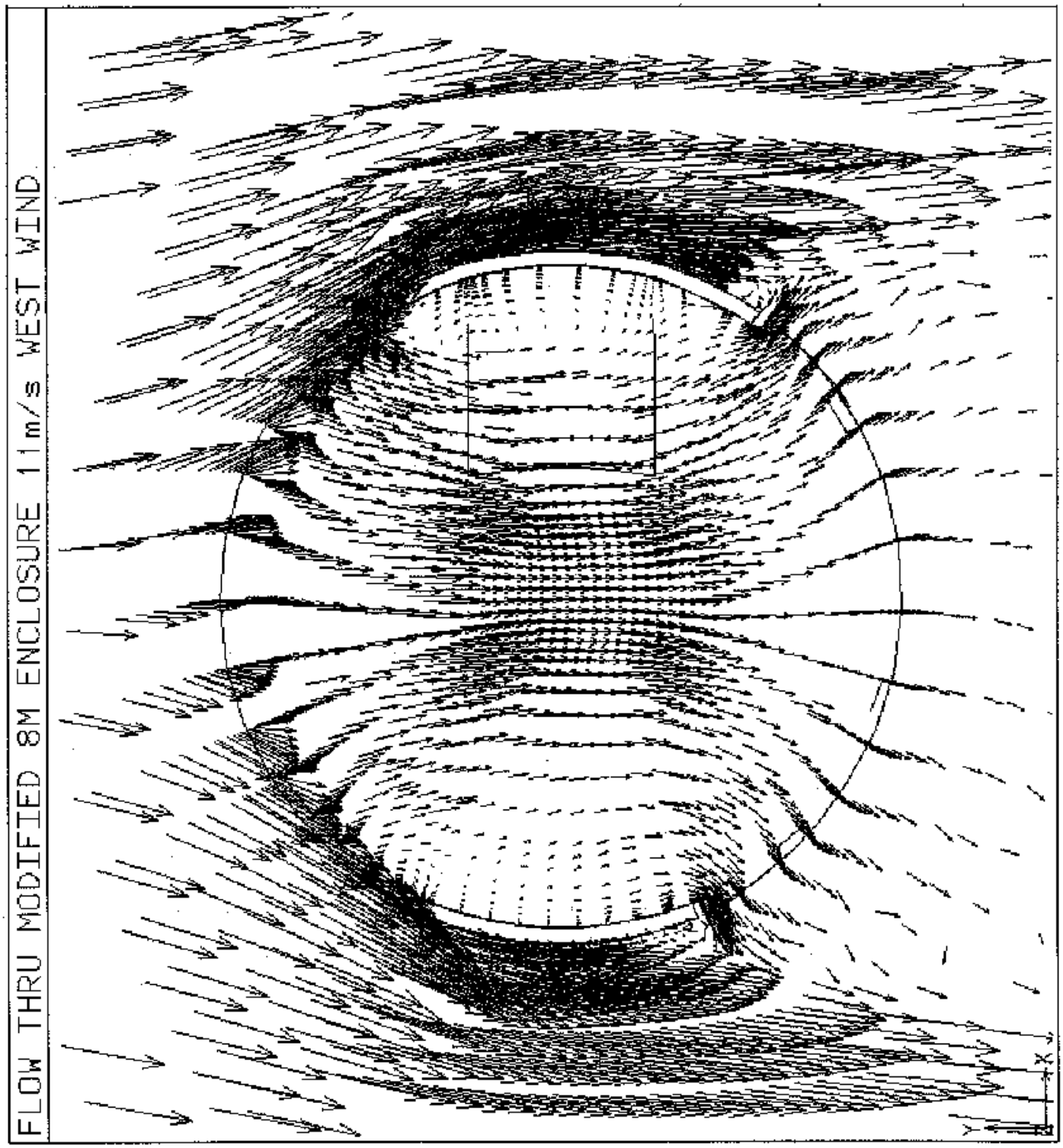

4

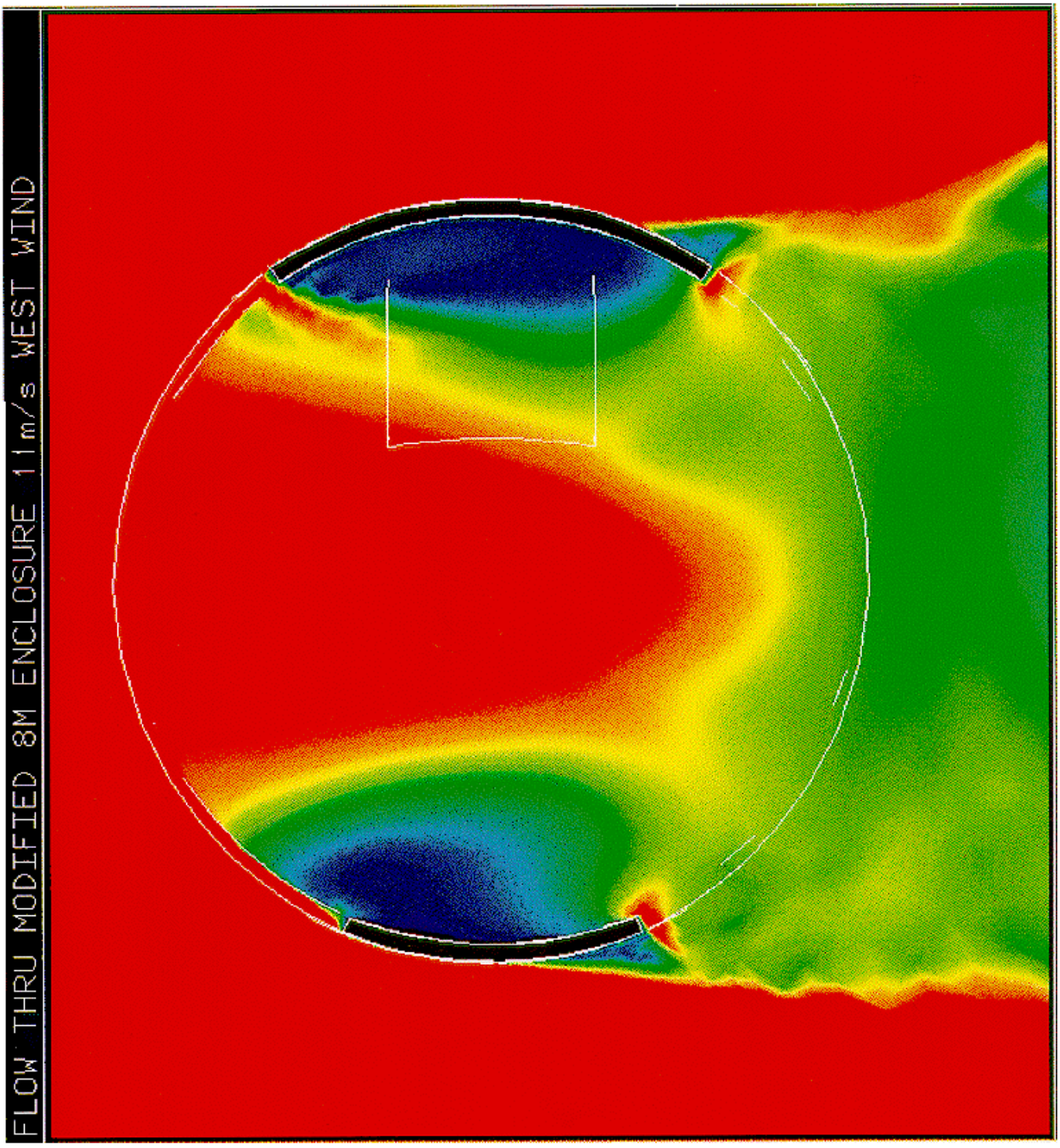

5

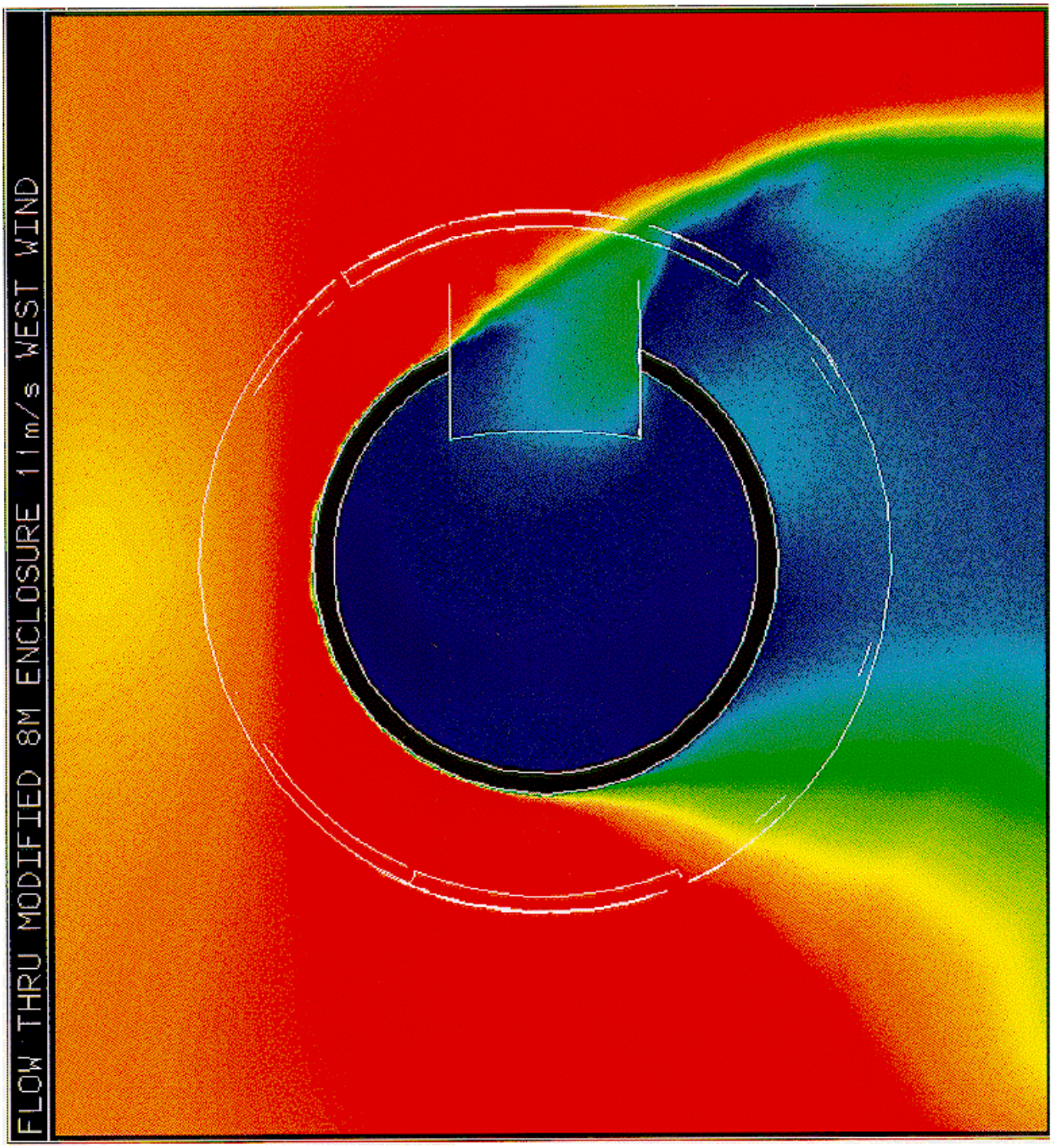

6

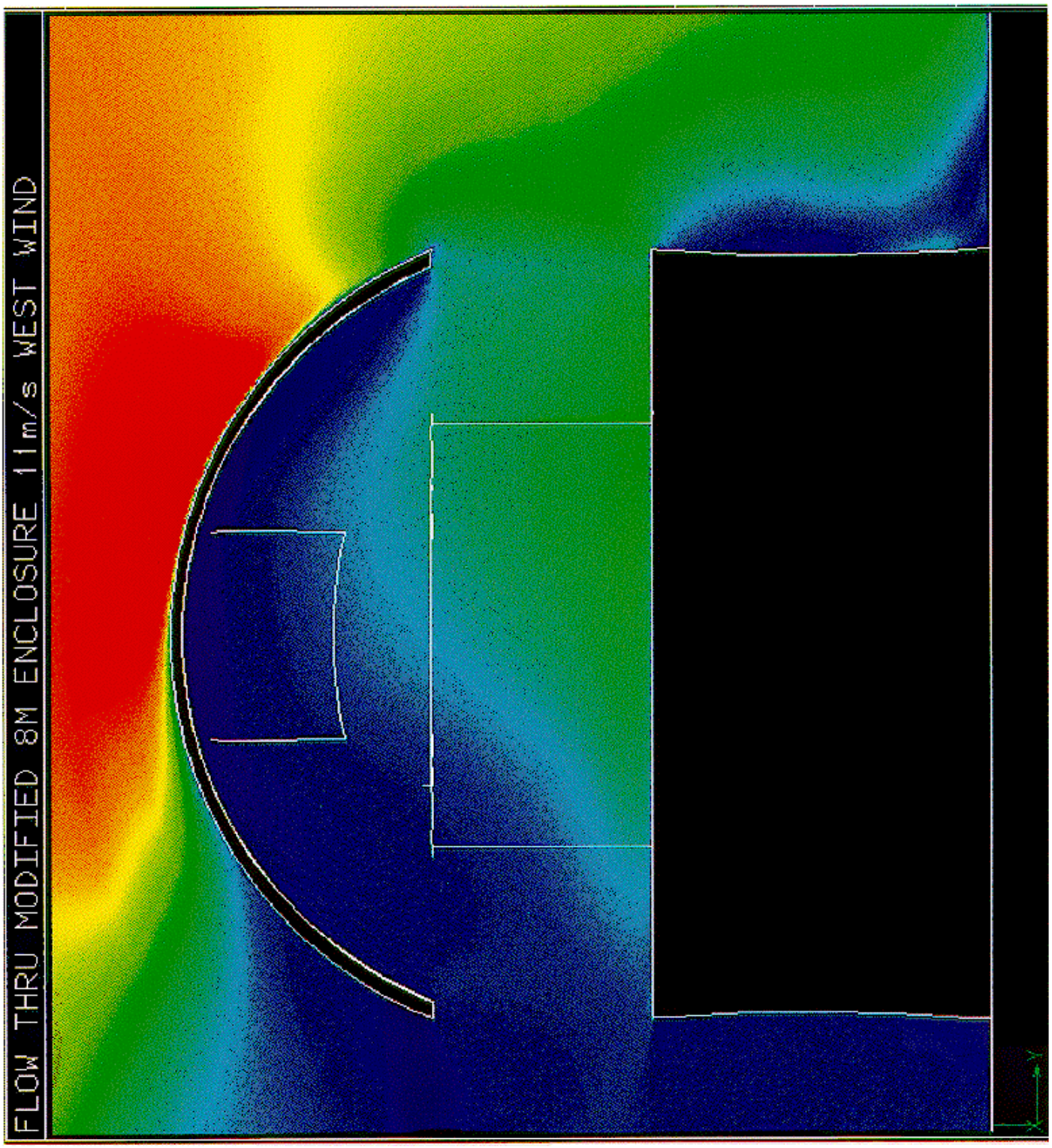

7

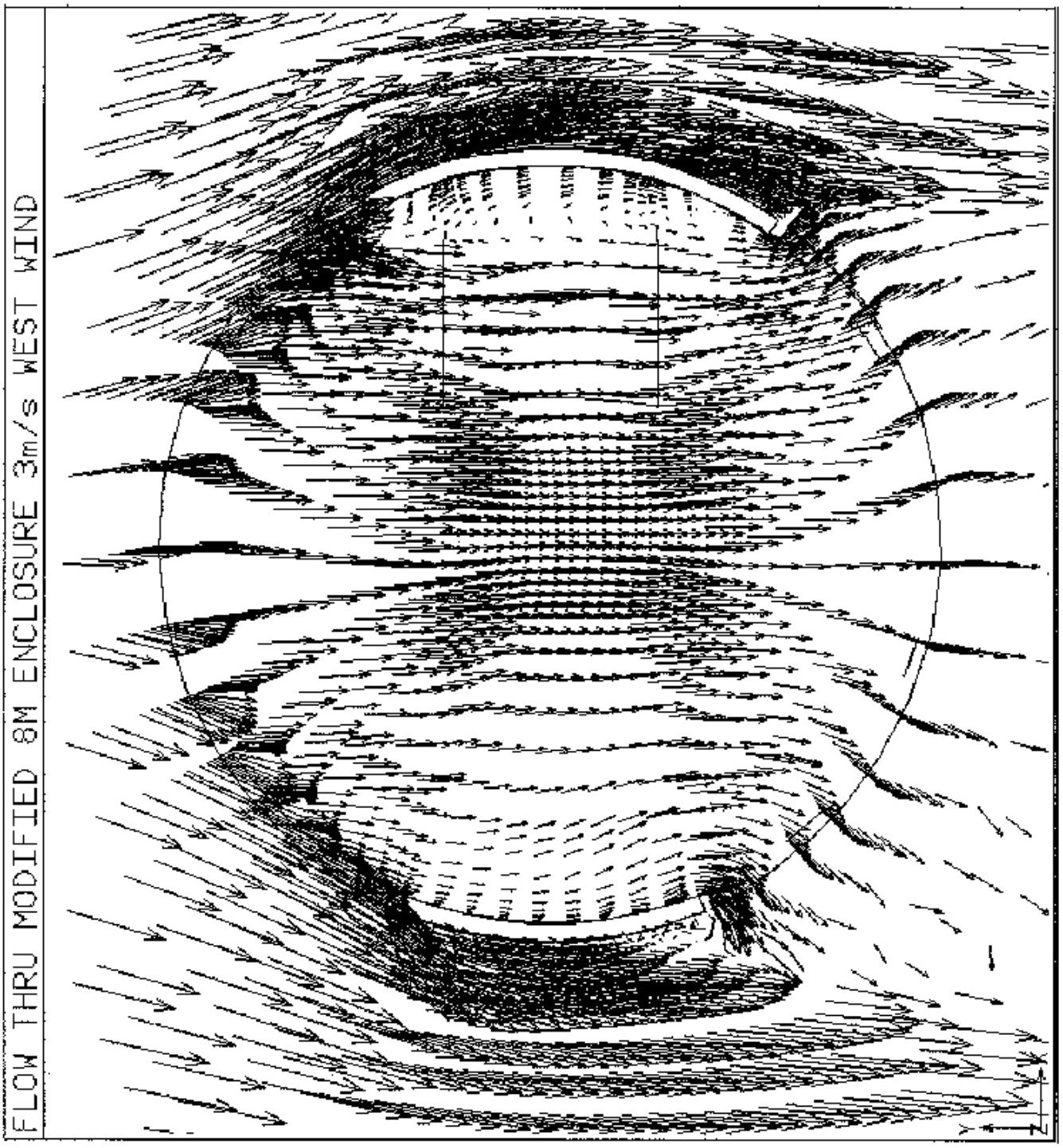

8

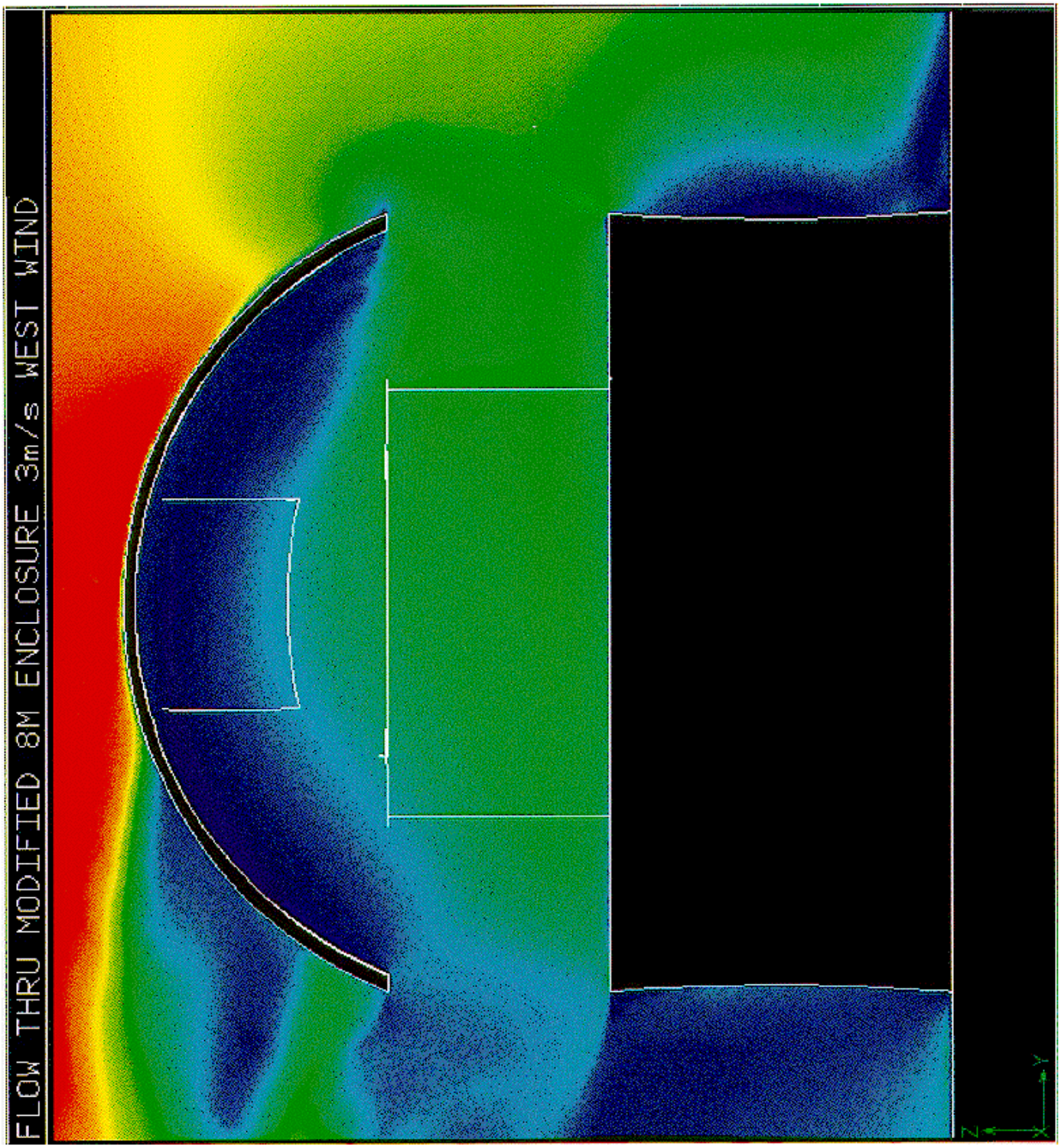

9

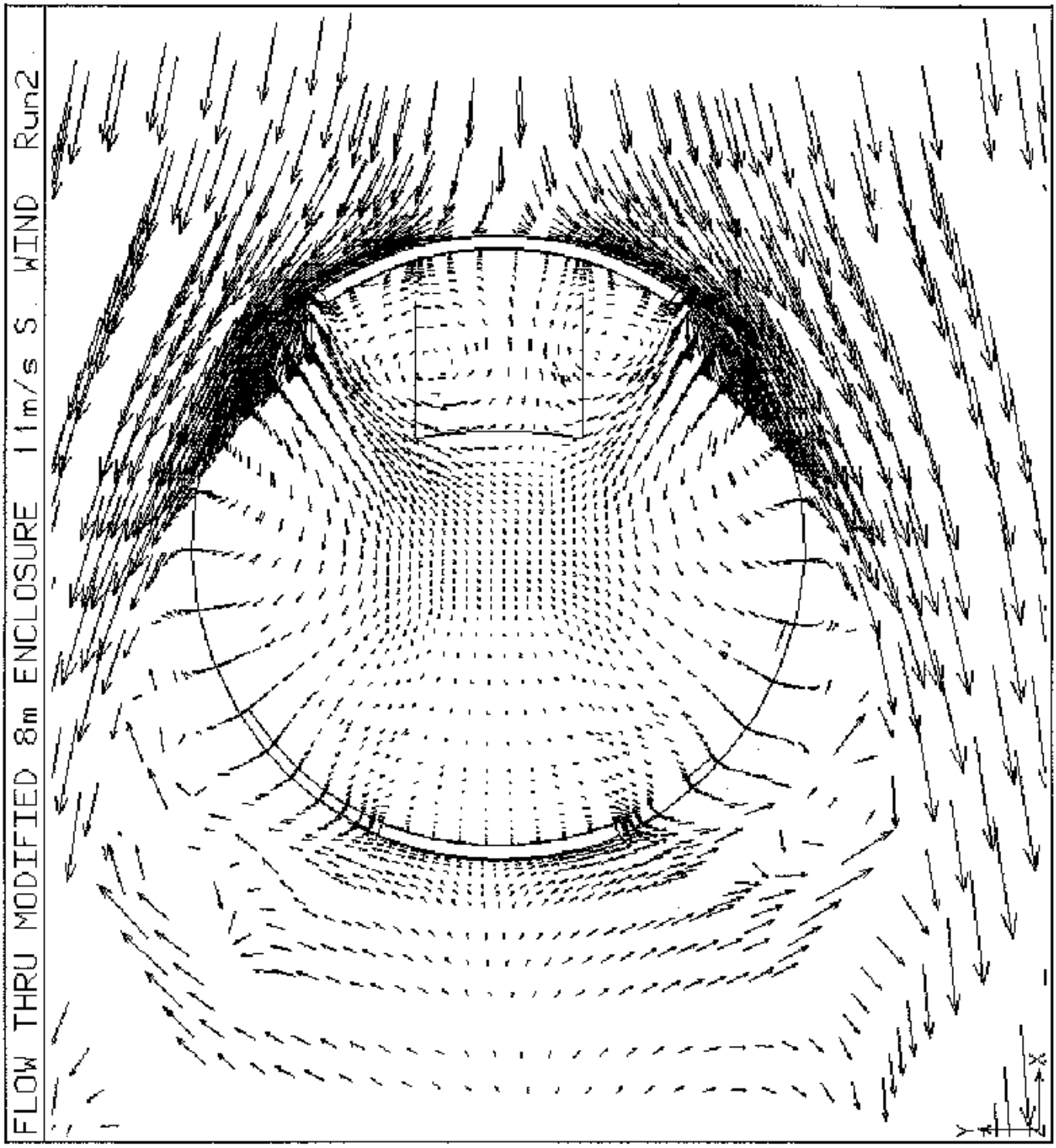

10

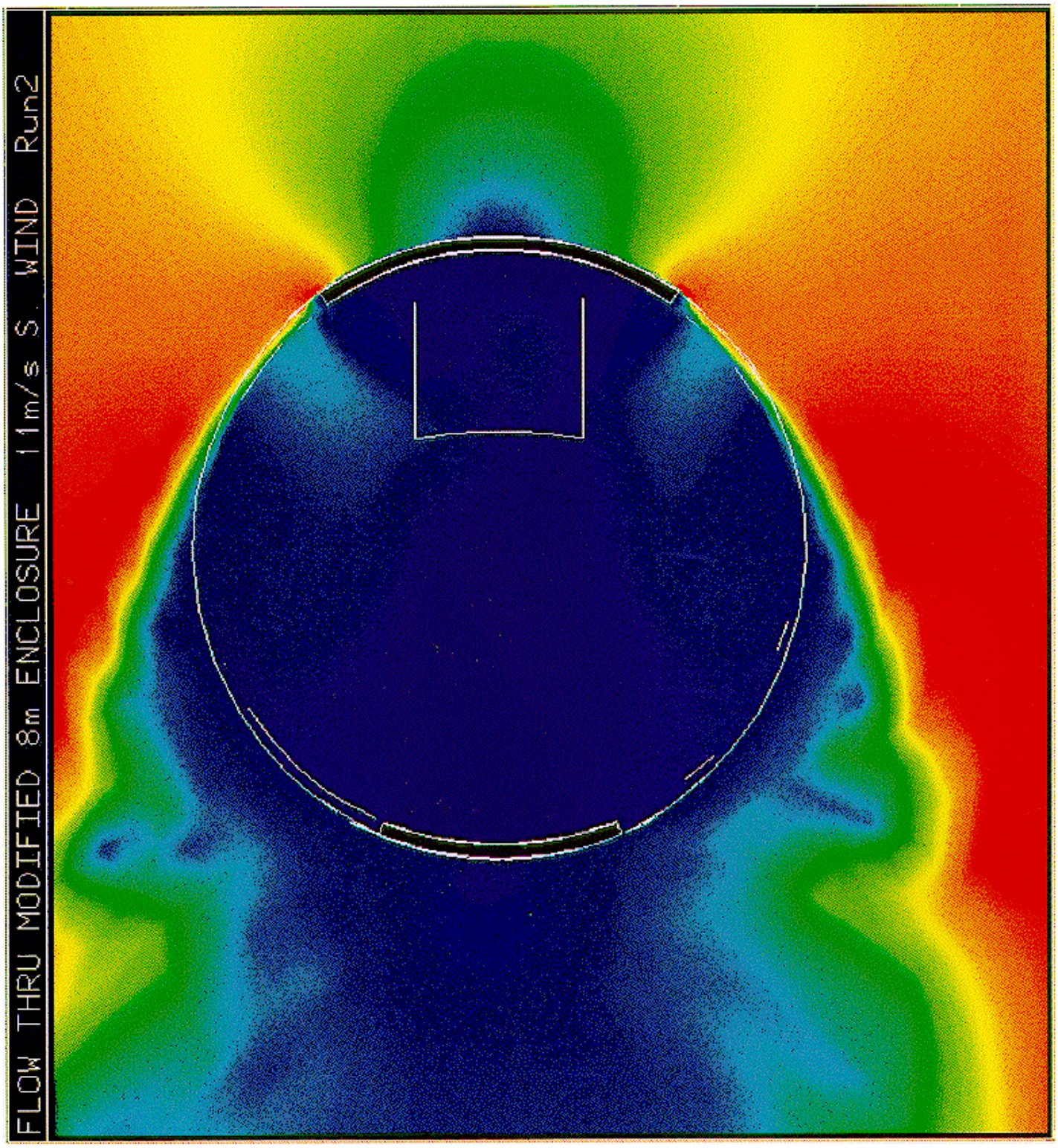

11

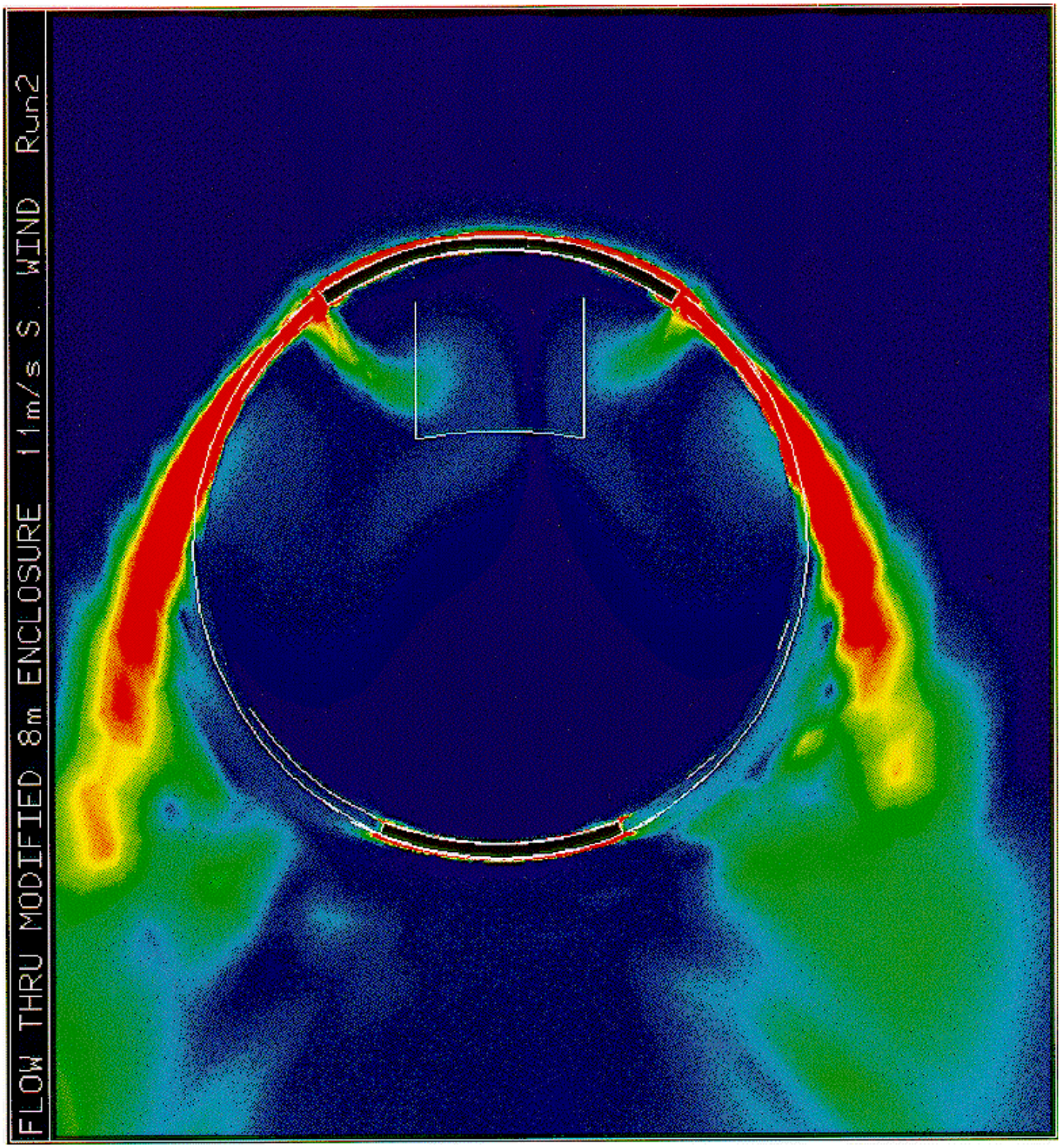

12

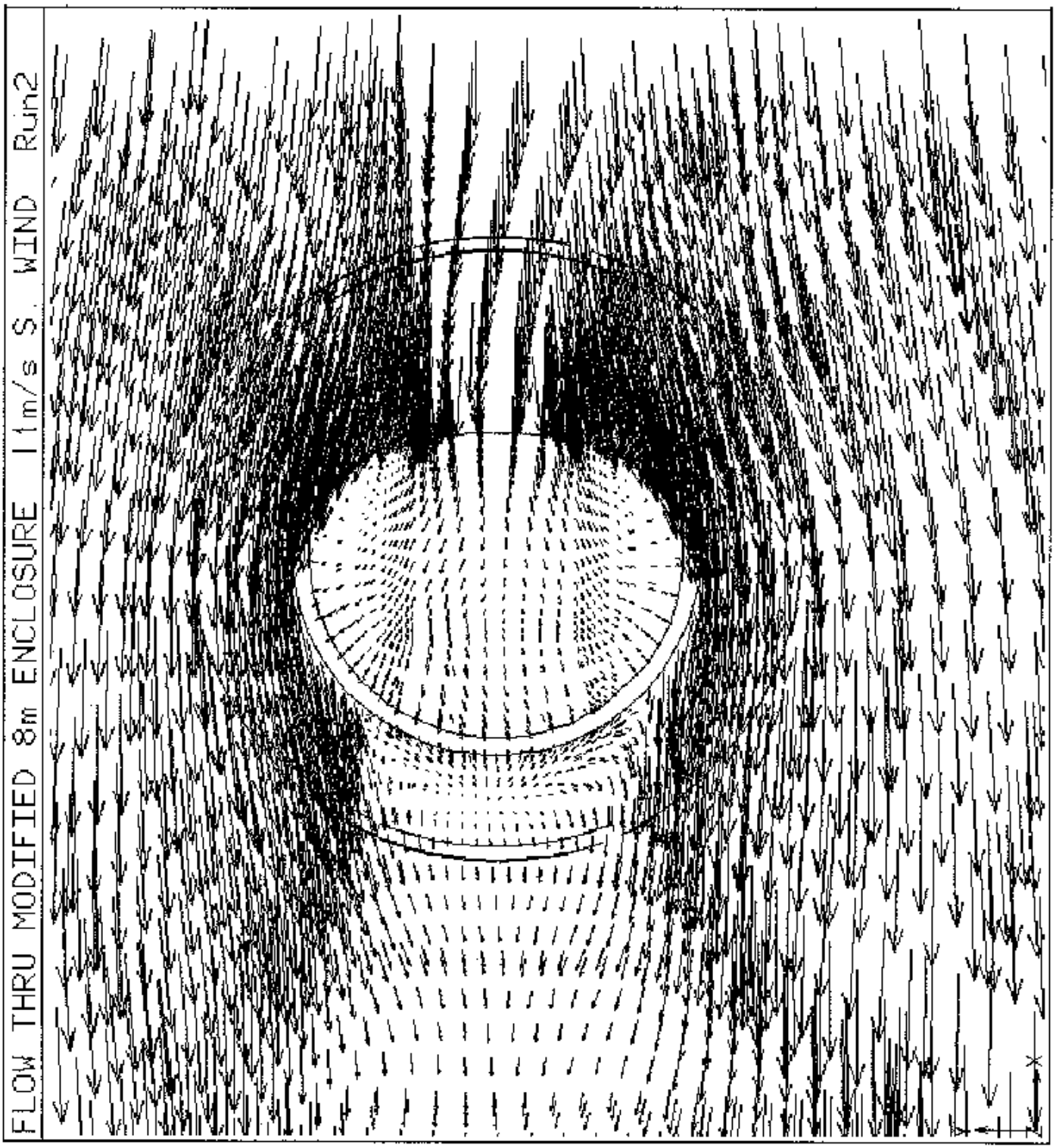

13

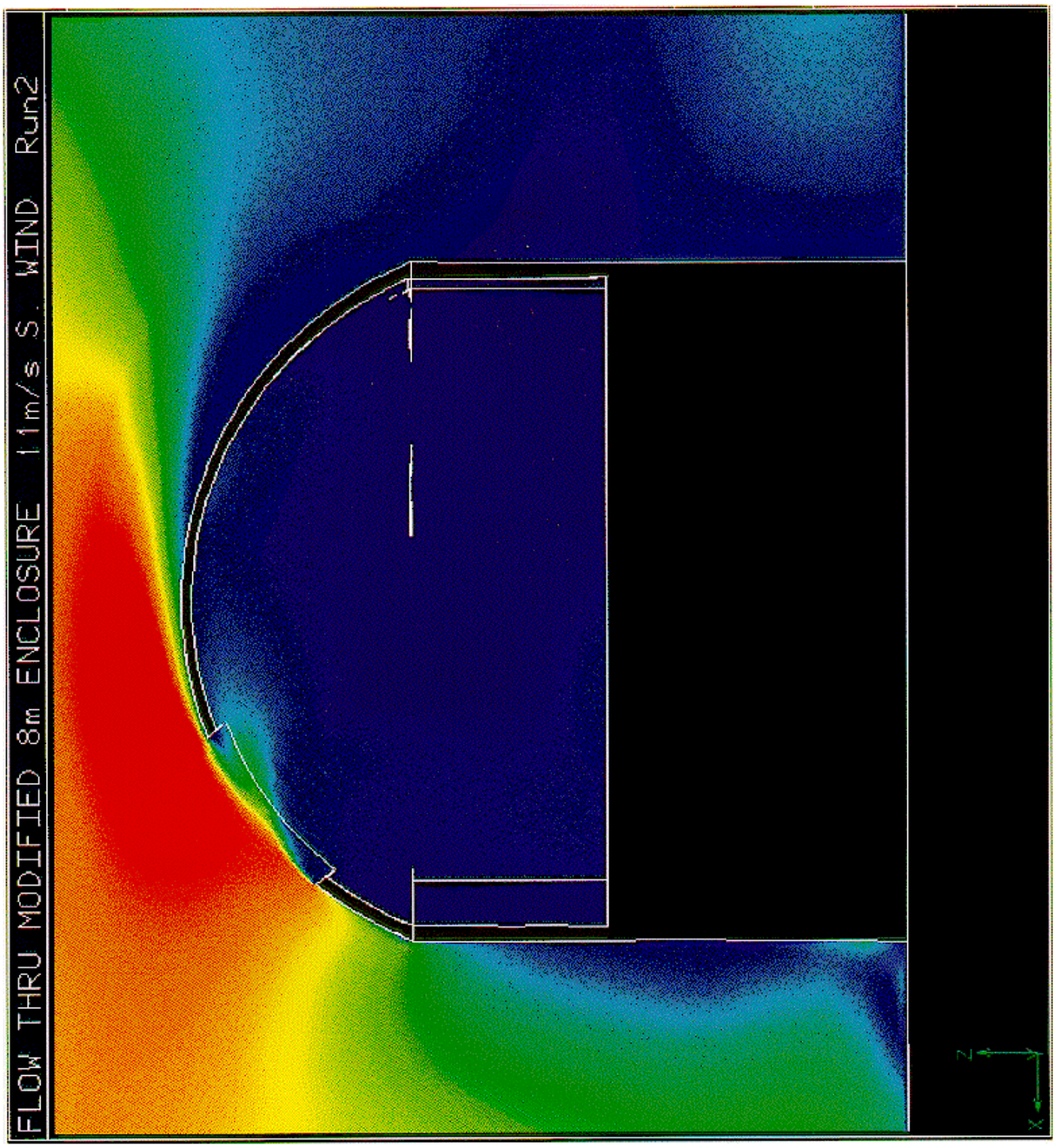
FLOW THRU MODIFIED 8m ENCLOSURE 11m/s S. WIND Run2
N
X

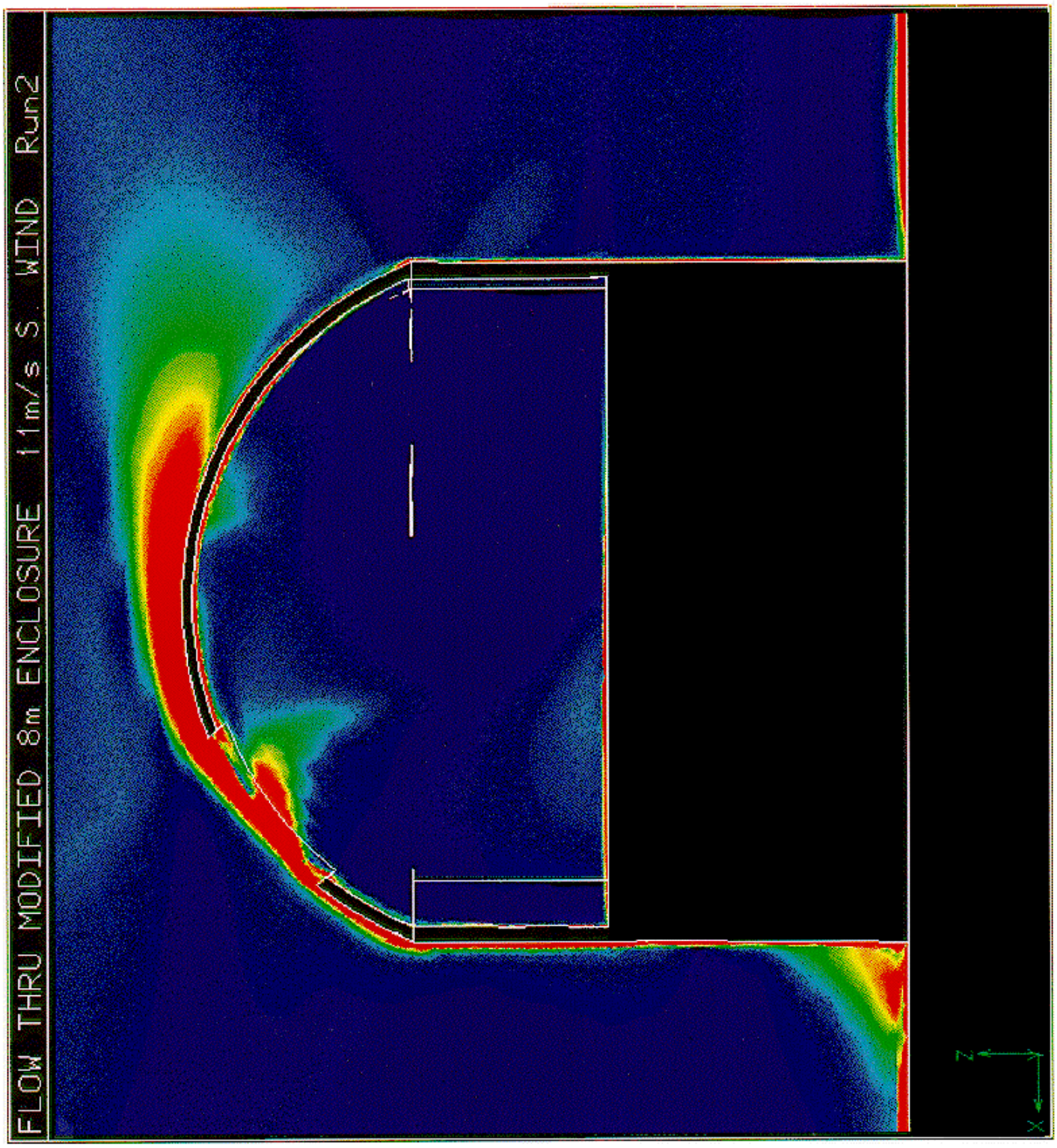

15

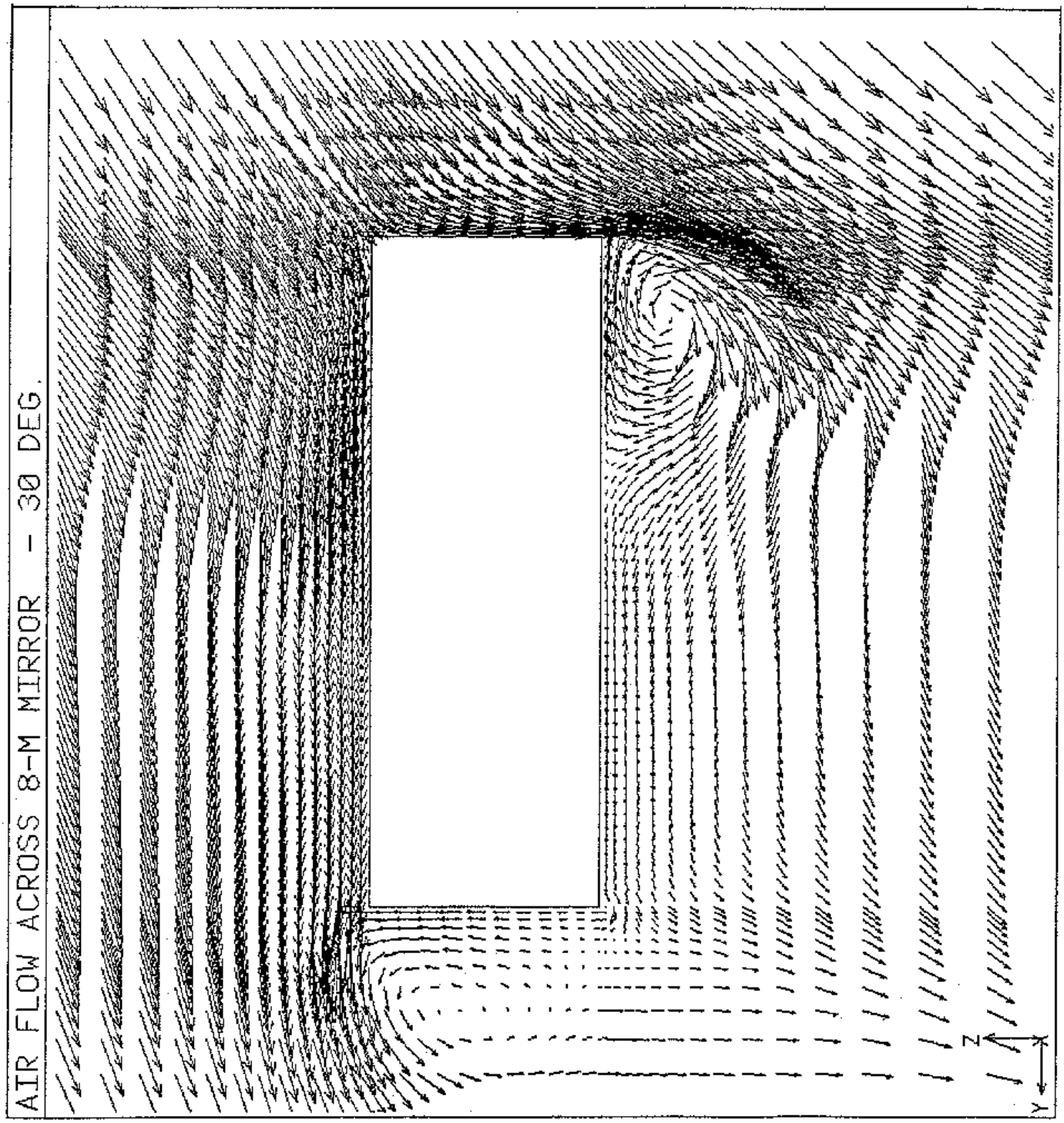

16

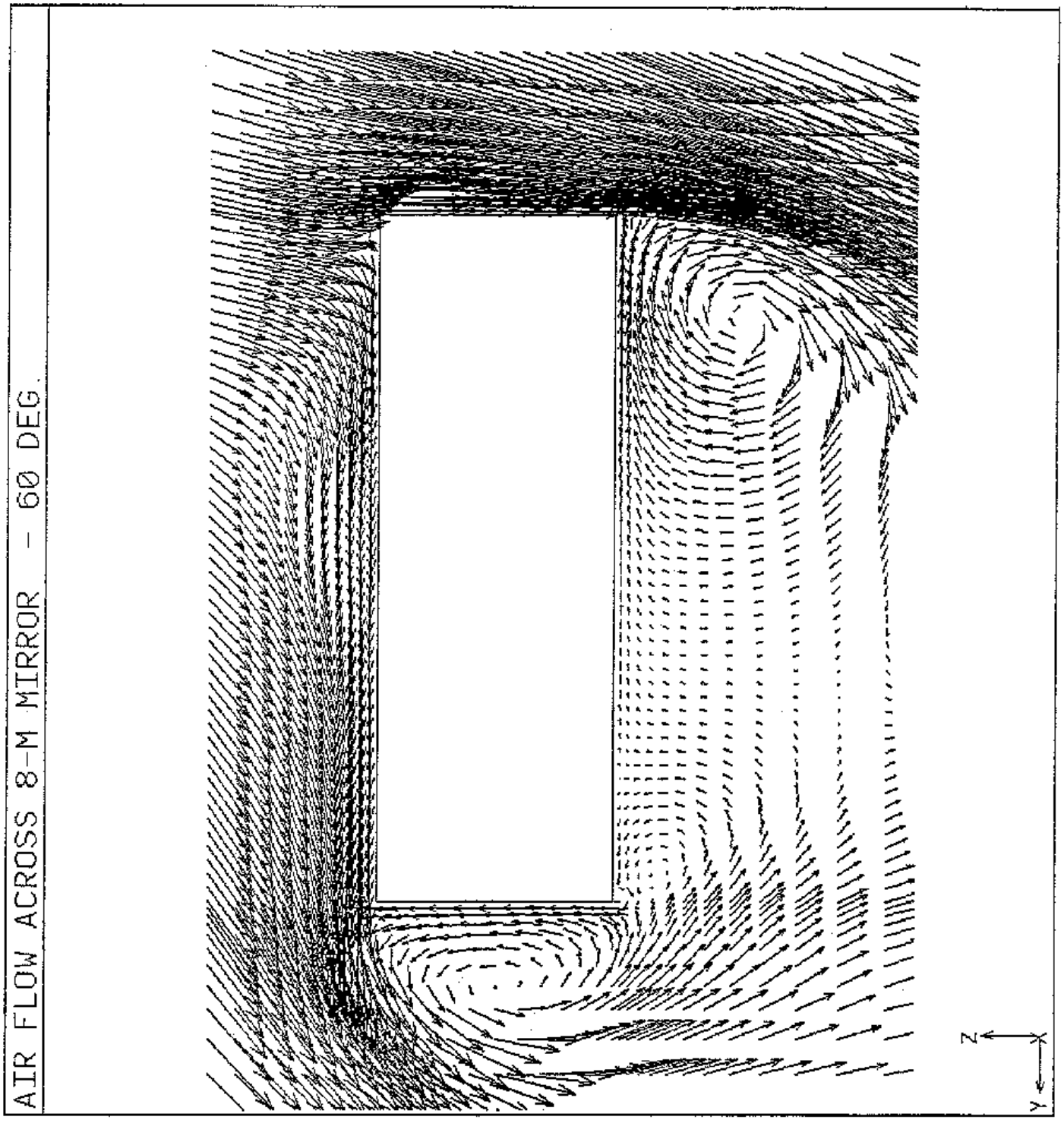

17

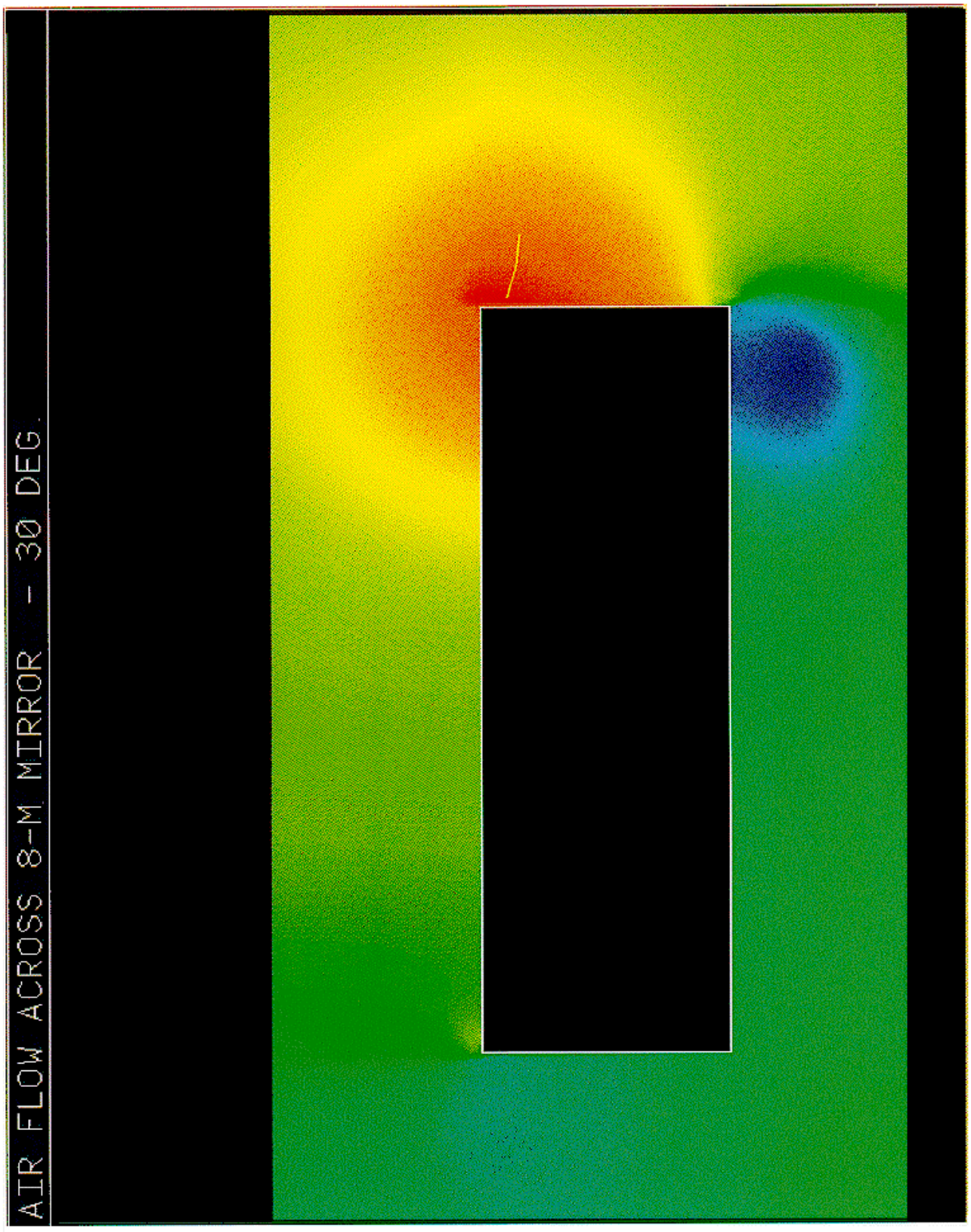

18a

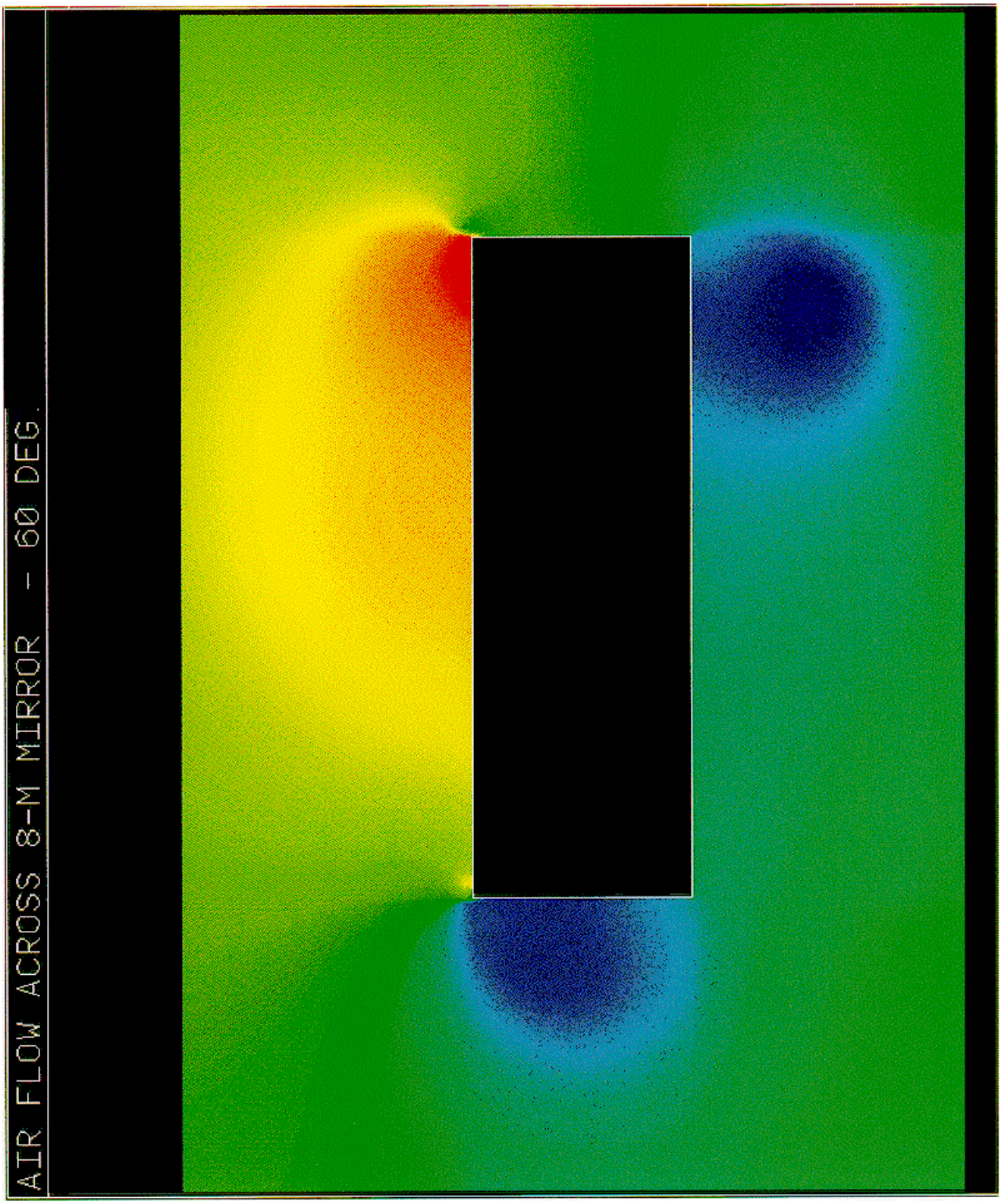

18b

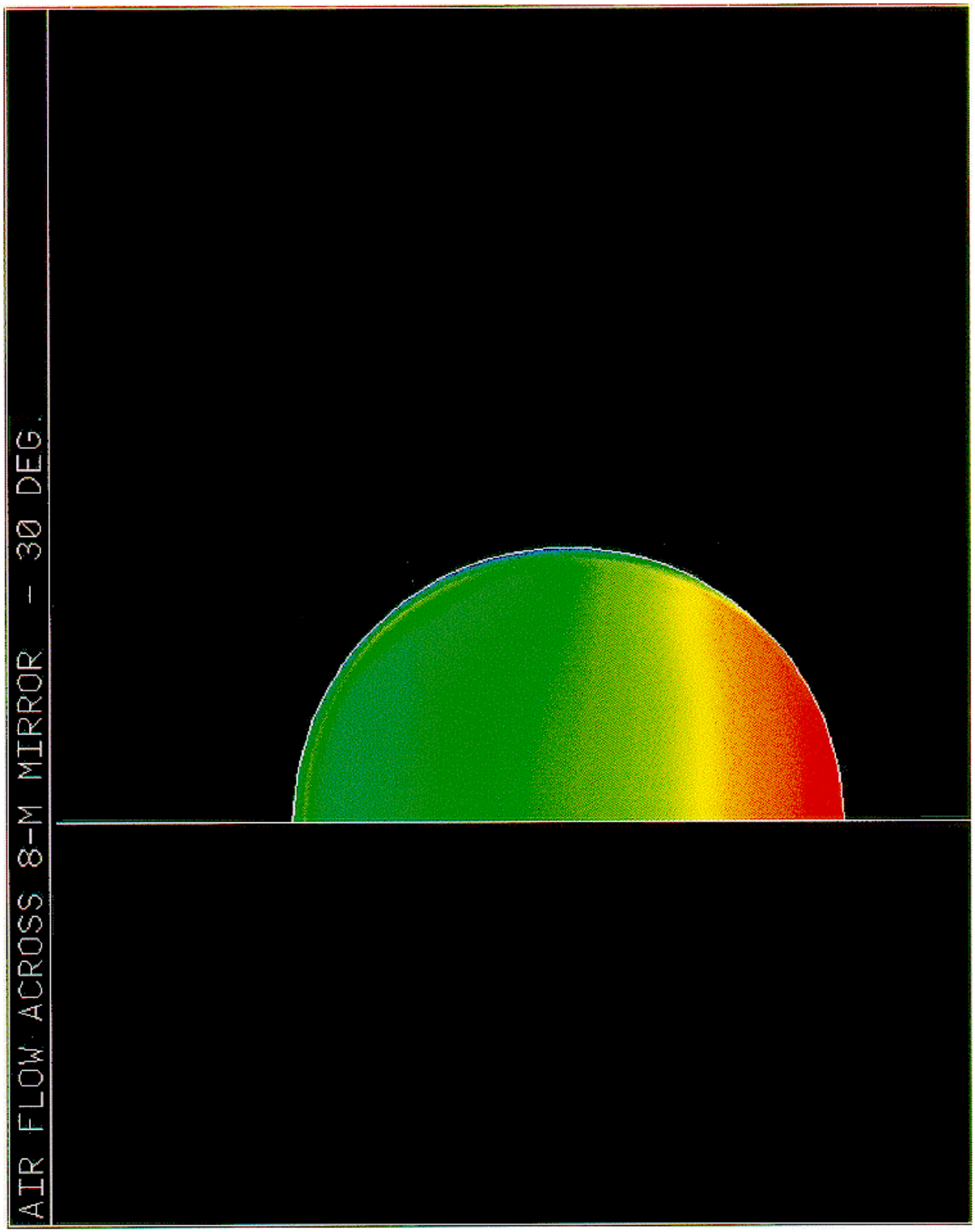

19a

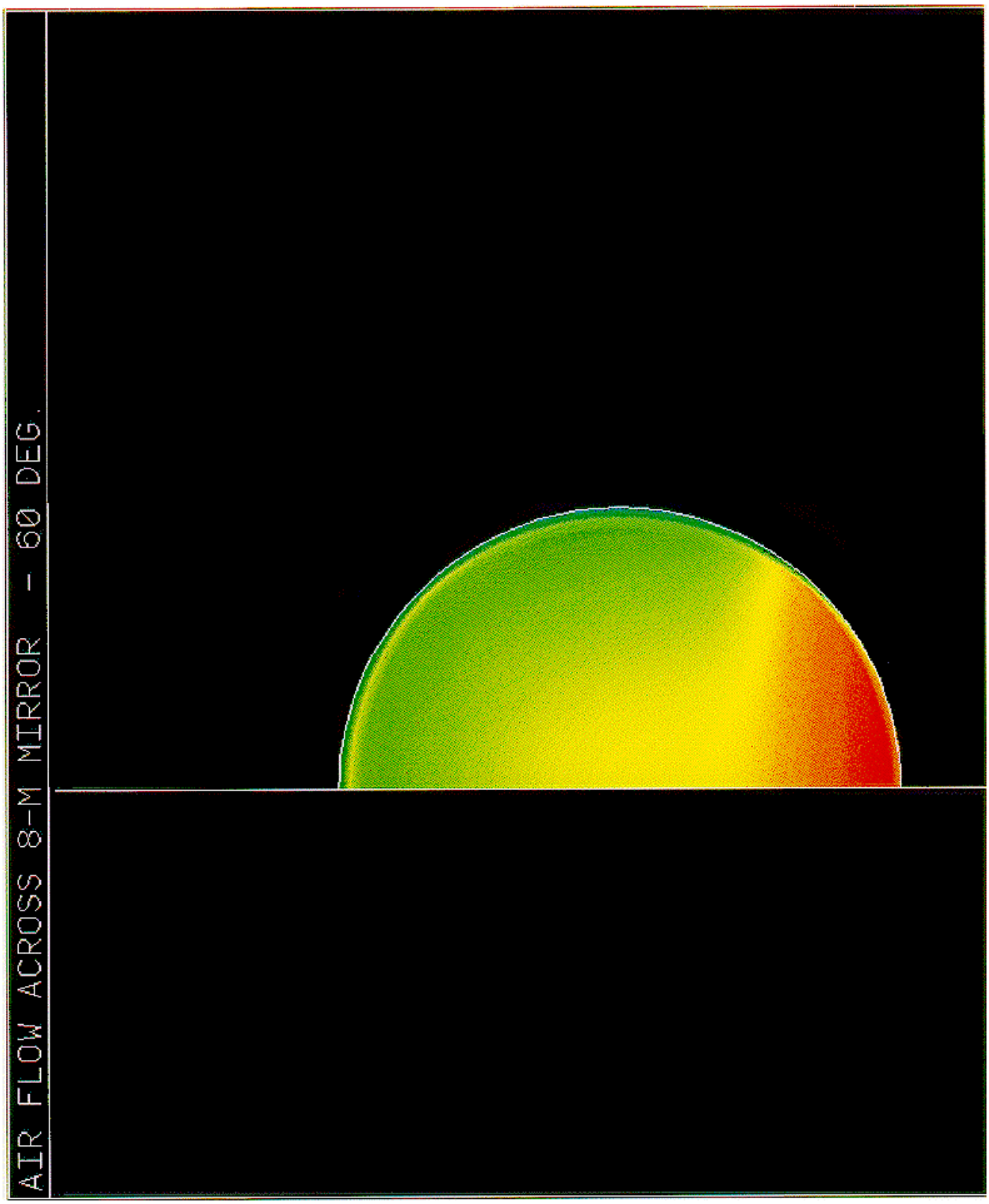

19b